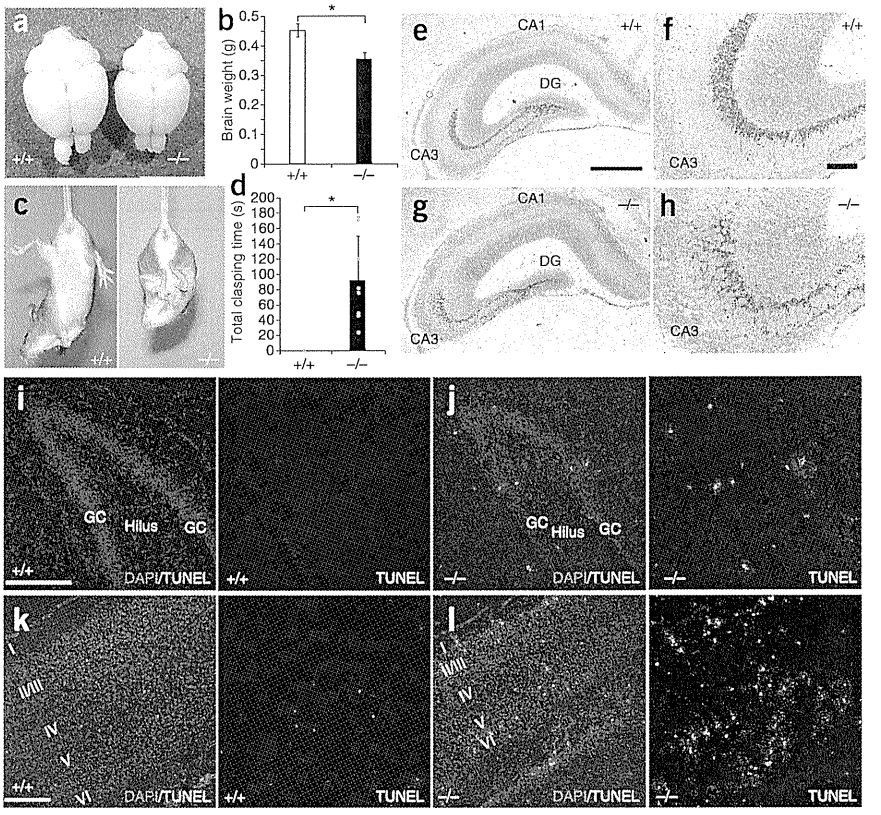


**Figure 4** *Rncr3*$^{-/-}$ mice exhibit neuronal dysfunction and aberrant growth of dentate granule cell axon. (**a**,**b**) Appearance of the brain and brain weight in wild-type and *Rncr3*$^{-/-}$ mice. Representative brains from wild-type (left) and *Rncr3*$^{-/-}$ mice (right, litter mates, 2 months old) are shown in **a**. Brain weights of wild-type ($n = 5$) and *Rncr3*$^{-/-}$ mice ($n = 9$) are shown in **b** (*$P < 0.001$). Error bars represent s.d. (**c**,**d**) Abnormal limb-clasping of *Rncr3*$^{-/-}$ mouse. A clasping response was observed in the *Rncr3*$^{-/-}$ mouse (**c**, right), but not in the wild-type mouse (**c**, left). Total clasping time was measured for 3 min (**d**). Error bars represent s.d. from the mean of $n = 4$ (wild type) and $n = 8$ (*Rncr3*$^{-/-}$). (**e**–**h**) Aberrant sprouting of mossy fibers in the *Rncr3*$^{-/-}$ mouse. The mossy fiber terminals were visualized by Timm staining with Nissl counterstaining at P10. Scale bars represent 500 μm (**e**,**g**) and 100 μm (**f**,**h**). (**i**,**j**) TUNEL assay of the P6 wild-type and *Rncr3*$^{-/-}$ dentate gyrus. Scale bars represent 200 μm. (**k**,**l**) TUNEL assay of the P6 wild-type and *Rncr3*$^{-/-}$ visual cortex. Scale bars represent 200 μm. GC, granule cell layer.

highly conserved miR-124a target sequence (**Fig. 5a**). We examined whether *Lhx2* is a target mRNA of miR-124a by constructing luciferase reporter plasmids that contained native or mutated seed sequences of the *Lhx2* 3′ UTR (**Fig. 5a**) and co-transfecting these reporter plasmids with miR-124a expression plasmids (*pBAsi-mU6-miR-124a-1*, *pBAsi-mU6-miR-124a-2* or *pBAsi-mU6-miR-124a-3*) into HEK 293T cells that lacked endogenous miR-124a (**Supplementary Fig. 8a**,**b**). HEK 293T cells transfected with miR-124a expression plasmids produced significant amounts of miR-124a ($P < 0.001$; **Supplementary Fig. 8a**,**b**). The luciferase activity of the native *Lhx2* 3′-UTR plasmid was significantly reduced by all of the pre-miR-124a expression plasmids ($P < 0.01$; **Fig. 5b**). However, luciferase activity of the mutated *Lhx2* 3′-UTR plasmid was not attenuated by miR-124a (**Fig. 5b**), and the luciferase mRNA levels of both native and mutated *Lhx2* 3′-UTR plasmids were not significantly reduced ($P < 0.004$; **Supplementary Fig. 8c**,**d**). We observed a statistically significant increase of luciferase activity in *Rncr3*$^{-/-}$ hippocampal neurons transfected with native Lhx2 3′-UTR plasmid ($P < 0.009$), but found no significant effect in neurons transfected with the mutated *Lhx2* 3′-UTR plasmid ($P > 0.45$; **Supplementary Fig. 8e**). Next, to determine whether *Lhx2* is an *in vivo* target of miR-124a, we performed immunostaining of the E17.5 *Rncr3*$^{-/-}$ retina using antibodies to LHX2 and TRβ2 antibodies (**Fig. 5c–e**). The number of LHX2 and TRβ2 double-positive cells was significantly increased in the *Rncr3*$^{-/-}$ retina compared with the wild-type retina ($P < 0.01$; **Fig. 5e**). We then introduced *Lhx2* expression plasmids that contained native or mutated 3′ UTR (*Lhx2-Nat* and *Lhx2-Mut*) together with an *egfp* expression plasmid into the P0 mouse retina by *in vivo* electroporation to determine whether retinal cell apoptosis occurs by *Lhx2* overexpression. The number of TUNEL-positive cells was increased in retina transfected with the *Lhx2-Mut* plasmid, but transfection with the *Lhx2-Nat* plasmid did not lead to an increase in the number of TUNEL-positive cells (**Fig. 5f–h**), suggesting that the native 3′ UTR was targeted by native miR-124a. This result is consistent with the observation that the number of TUNEL-positive cells was significantly increased in the *Rncr3*$^{-/-}$ retina ($P < 0.05$; **Supplementary Fig. 6a–c**). These results suggest that *Lhx2* mRNA is a miR-124a target in the retina and that downregulation of *Lhx2* mRNA by miR-124a is necessary for retinal cell survival.

*Lhx2* is known to be required for hippocampal formation[24]. We therefore conducted immunostaining on the dentate gyrus with antibodies to LHX2 and the dentate gyrus marker PROX1. The number of LHX2 and PROX1 double-positive cells was significantly increased in the *Rncr3*$^{-/-}$ dentate gyrus ($P < 0.001$; **Fig. 5i–k**). Furthermore, we compared the expression of *Rncr3* and *Lhx2* mRNA and LHX2 protein in the E12.5 forebrain and P3 retina (**Supplementary Fig. 8f–o**). At E12.5, *Lhx2* mRNA was highly expressed in both the hippocampus and thalamus, whereas *Rncr3* was highly expressed only in the thalamus. In both the developing brain and retina, LHX2 protein was not expressed in regions in which both *Lhx2* and *Rncr3* mRNA were expressed, suggesting that miR-124a targets *Lhx2* mRNA both in the retina and the brain and that miR-124a inhibits translation of *Lhx2* mRNA. Cell density was significantly higher in the dentate gyrus in *Rncr3*$^{-/-}$ mice than in wild-type mice, as determined by counting PROX1-positive cells ($P < 0.004$; **Fig. 5i**,**j**,**l**). To assess the role of *Lhx2* in aberrant mossy fiber sprouting, we electroporated *Lhx2-Nat* and *Lhx2-Mut* plasmids into primary cultured hippocampal cells. Substantial neurite extension was observed in cells expressing *Lhx2-Mut* (**Fig. 5m–o**). To evaluate axonal elongation in dentate granule cells, we immunostained hippocampal PROX1 neurons and then measured the axonal length of PROX1-positive cells (**Fig. 5p**,**q**). The percentage of neurons that contained longer axons, greater than 150 μm in length, was increased by expression of *Lhx2-Mut* (**Fig. 5p**). Furthermore, the average length of the neurons in the top 25$^{th}$ percentile of the population was also significantly increased in *Lhx2-Mut*–expression neurons ($P < 0.05$; **Fig. 5q**). We ectopically expressed *Lhx2* using lentivirus in P6 rat dentate gyrus in slice culture and found that *Lhx2*-transduced dentate granule cells extended longer

axons to the CA3 region by 5 d *in vitro* (DIV) than the wild-type cells (**Fig. 5r–u**). These results suggest that a proper LHX2 protein level, which is affected by miR-124a, is required for the appropriate development of axons in the dentate gyrus.

### Rescue of *Rncr3*$^{-/-}$ mice by pre-miR-124a-2 or *Lhx2* knockdown

To determine whether miR-124a is responsible for the *Rncr3*$^{-/-}$ retinal phenotype, we carried out a rescue experiment by mating *Rncr3*$^{-/-}$ mice with transgenic mice that specifically expressed miR-124a in

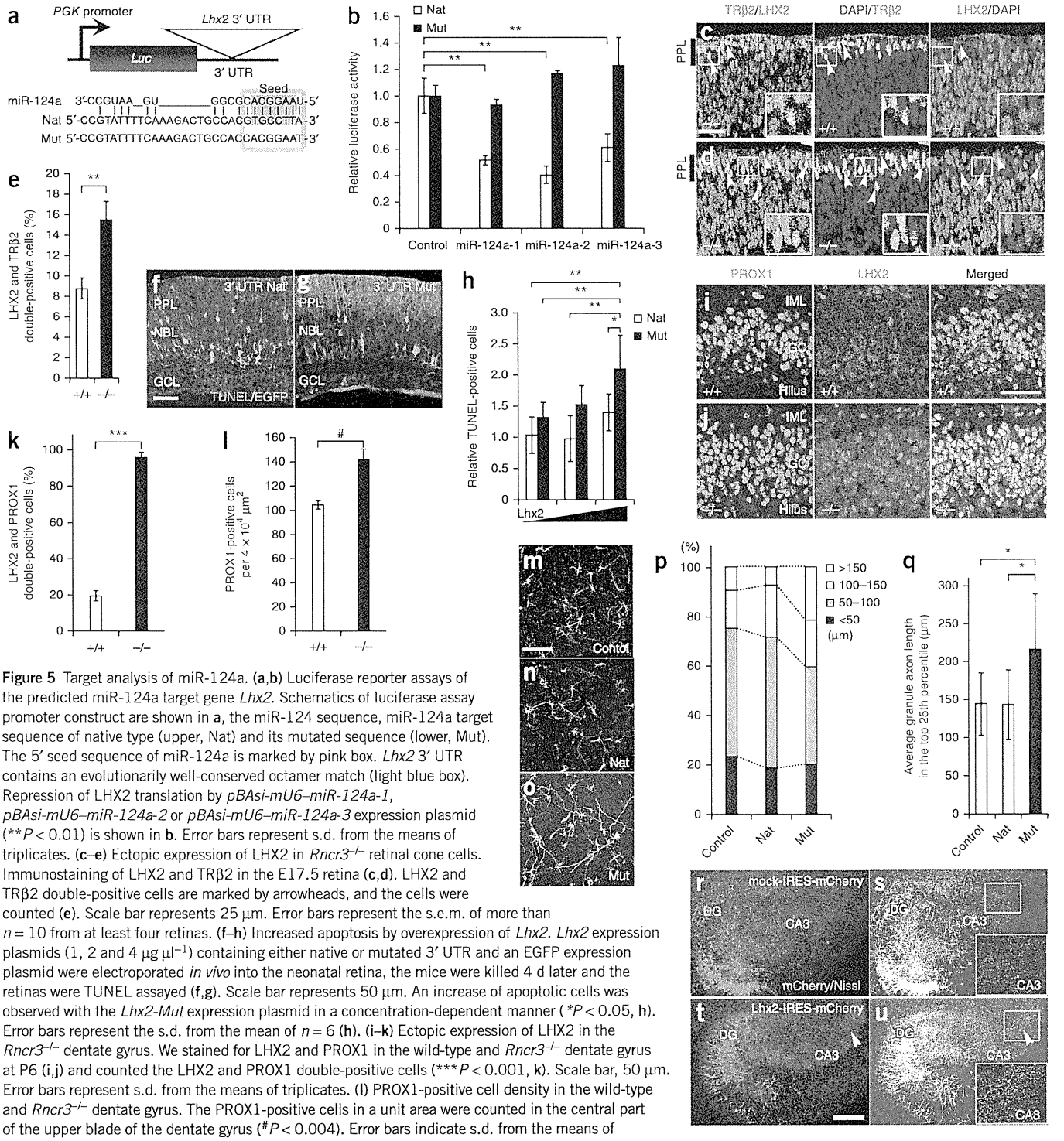


**Figure 5** Target analysis of miR-124a. (**a**,**b**) Luciferase reporter assays of the predicted miR-124a target gene *Lhx2*. Schematics of luciferase assay promoter construct are shown in **a**, the miR-124 sequence, miR-124a target sequence of native type (upper, Nat) and its mutated sequence (lower, Mut). The 5′ seed sequence of miR-124a is marked by pink box. *Lhx2* 3′ UTR contains an evolutionarily well-conserved octamer match (light blue box). Repression of LHX2 translation by *pBAsi-mU6–miR-124a-1*, *pBAsi-mU6–miR-124a-2* or *pBAsi-mU6–miR-124a-3* expression plasmid (**$P < 0.01$) is shown in **b**. Error bars represent s.d. from the means of triplicates. (**c**–**e**) Ectopic expression of LHX2 in *Rncr3*$^{-/-}$ retinal cone cells. Immunostaining of LHX2 and TRβ2 in the E17.5 retina (**c**,**d**). LHX2 and TRβ2 double-positive cells are marked by arrowheads, and the cells were counted (**e**). Scale bar represents 25 μm. Error bars represent the s.e.m. of more than $n = 10$ from at least four retinas. (**f**–**h**) Increased apoptosis by overexpression of *Lhx2*. *Lhx2* expression plasmids (1, 2 and 4 μg μl$^{-1}$) containing either native or mutated 3′ UTR and an EGFP expression plasmid were electroporated *in vivo* into the neonatal retina, the mice were killed 4 d later and the retinas were TUNEL assayed (**f**,**g**). Scale bar represents 50 μm. An increase of apoptotic cells was observed with the *Lhx2-Mut* expression plasmid in a concentration-dependent manner (*$P < 0.05$, **h**). Error bars represent the s.d. from the mean of $n = 6$ (**h**). (**i**–**k**) Ectopic expression of LHX2 in the *Rncr3*$^{-/-}$ dentate gyrus. We stained for LHX2 and PROX1 in the wild-type and *Rncr3*$^{-/-}$ dentate gyrus at P6 (**i**,**j**) and counted the LHX2 and PROX1 double-positive cells (***$P < 0.001$, **k**). Scale bar, 50 μm. Error bars represent s.d. from the means of triplicates. (**l**) PROX1-positive cell density in the wild-type and *Rncr3*$^{-/-}$ dentate gyrus. The PROX1-positive cells in a unit area were counted in the central part of the upper blade of the dentate gyrus (#$P < 0.004$). Error bars indicate s.d. from the means of triplicates. (**m**–**q**) Axonal extension in *Lhx2-Mut*–expressing neurons. Primary hippocampal neurons from P0 mouse were transfected with mock (control), *Lhx2-Nat* (native), *Lhx2-Mut* (mutated) together with EGFP by electroporation. Confocal microimages of neurons 72 h after transfection are shown in **m**–**o**. Scale bar represents 200 μm. The percentages of axons with lengths ≤50, 50–100, 100–150 and >150 μm from $n = 85$ (control), 81 (nat), and 89 (mut) neurons are shown in **p**. The average axon lengths in the top 25% percentile are shown in **q**. Error bars represent s.d. (**r**–**u**) Lentivirus-infected hippocampal slice culture. Shown are confocal images of the P6, 5 DIV sliced rat hippocampus infected with mock (control, **r**,**s**) or *Lhx2* (**t**,**u**) expression virus. The small white boxes in **s** and **u** are the CA3 regions, magnified in the bottom right corner. Arrowheads indicate elongated mossy fibers in the CA3. Scale bar represents 200 μm. IML, inner molecular layer.

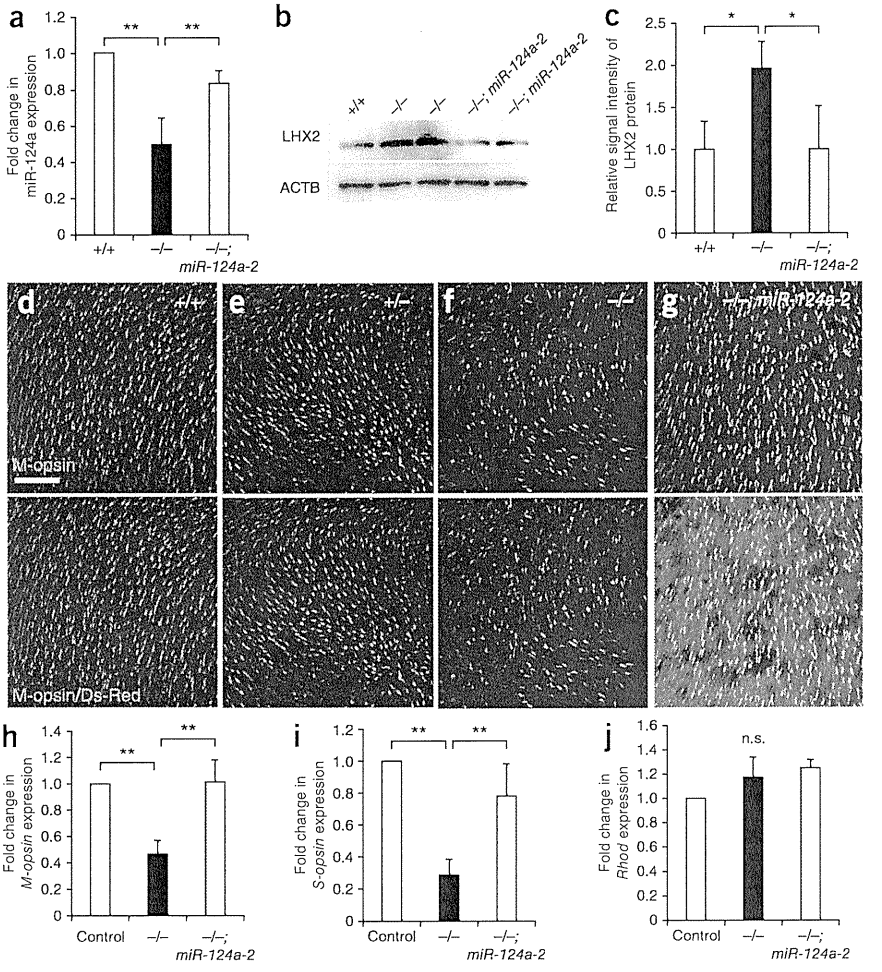


**Figure 6** *In vivo* rescue experiments of *Rncr3*$^{-/-}$ mice by miR-124a expression in the retina. (**a**) Expression of miR-124a in the wild-type, *Rncr3*$^{-/-}$ and *Rncr3*$^{-/-}$*; Crx–miR-124a-2* retinas (**$P < 0.01$). Error bars represent the s.d. from the mean of triplicate (wild type and *Rncr3*$^{-/-}$) and $n = 4$ (*Rncr3*$^{-/-}$*; Crx–miR-124a-2*). (**b**,**c**) Comparison of LHX2 protein levels in the wild-type, *Rncr3*$^{-/-}$ and *Rncr3*$^{-/-}$*; Crx–miR-124a-2* retina. Western blots of LHX2 in the retina are shown in **b**. ACTB (β-actin) was used as a loading control. The signal intensity of LHX2 protein is shown in **c** (*$P < 0.05$). Error bars represent the s.d. from the means of triplicates (wild type) and $n = 4$ (*Rncr3*$^{-/-}$ and *Rncr3*$^{-/-}$*; Crx–miR-124a-2*). (**d–g**) Rescue of decreased cone cells by miR-124a expression. Flat-mount immunostaining using antibody to M-opsin (green). The *pre-miR-124a-2* transgene also expressed Ds-Red (magenta) as a marker. Scale bar represents 50 μm. (**h–j**) Real-time qRT-PCR analysis of control (+/+*; Crx–miR-124a-2* and *Rncr3*$^{+/-}$*; Crx–miR-124a-2*), *Rncr3*$^{-/-}$ and *Rncr3*$^{-/-}$*; Crx–miR-124a-2* transgenic retinas. Intron-spanning primers amplifying mouse *M-opsin* (also known as *Opn1mw*, **h**), *S-opsin* (also known as *Opn1sw*, **i**), *Rho* (**j**), and *Actb* were used for normalization. Error bars represent the s.d. from the means of three independent littermate pairs. **$P < 0.01$; n.s., not significant, $P > 0.05$.

photoreceptor cells using a *Ds-Red-intron-miR-124a-2* expression cassette driven by 2.3 kb of the *Crx* promoter[5,25] (*Crx–miR-124a-2*; **Supplementary Fig. 9a**). In the P1 retina, we observed that both miR-124a expression and the LHX2 protein level reverted back to those of control mice (**Fig. 6a–c**). We then performed flat-mount immunostaining (**Fig. 6d–g**) and conducted qPCR analysis on retinal photoreceptor marker genes using the adult retina (**Fig. 6h–j**). Both the decreased cone cell numbers and gene expression in the *Rncr3*$^{-/-}$ retina were restored to normal levels when transgenic pre-miR-124a-2 was expressed (**Fig. 6d–i**). The number of mislocalized cone cells also recovered (**Supplementary Fig. 9b–i**). These results suggest that the cone cell reduction and mislocalization in the *Rncr3*$^{-/-}$ retina are the results of miR-124a-1 disruption and that the primary function of *Rncr3* is to encode miR-124a.

To determine whether the loss of miR-124a is also responsible for the brain phenotypes, we generated a transgenic mouse that expresses *Ds-Red-intron-miR-124a-2* in postmitotic neurons, driven by 4.3 kb of the *synapsin 1* promoter (*Syn1–miR-124a-2*)[26] (**Supplementary Fig. 10a–c**). We performed an *in situ* hybridization of miR-124a and immunostained for LHX2 in the P10 brain. In the dentate gyrus of the *Rncr3*$^{-/-}$*; Syn1–miR-124a-2* mice, both the reduced level of mature miR-124a and the elevated level of LHX2 protein that we observed in *Rncr3*$^{-/-}$ mice were restored to similar levels as seen in control mice (**Fig. 7a–f**). In addition, the number of apoptotic cells was significantly reduced in the brains of *Rncr3*$^{-/-}$*; Syn1–miR-124a-2* mice compared with *Rncr3*$^{-/-}$ mice ($P < 0.01$; **Supplementary Fig. 10d**). In *Rncr3*$^{-/-}$*; Syn1–miR-124a-2* mice, Timm-stained mossy fiber axonal terminals incompletely, but substantially, recovered from aberrant sprouting into the CA3 region (**Fig. 7g–l**). The other phenotypes, including brain weight, clasping and apoptosis in the cortex, were not substantially rescued in *Rncr3*$^{-/-}$*; Syn1–miR-124a-2* mice (data not shown). This partial rescue may be a result of insufficient expression and/or inappropriate expression timing of the miR-124a transgene.

To determine whether downregulation of *Lhx2* can rescue the *Rncr3*$^{-/-}$ phenotype, we constructed a short hairpin RNA (shRNA) to knockdown *Lhx2* (*shLhx2*; **Supplementary Fig. 11a,b**). We transfected *shLhx2* into organ-cultured P0 retina using a recombinant adeno-associated virus serotype 5 (AAV5; **Supplementary Fig. 11c**). After 5 DIV, we performed immunostaining using an antibody to S-opsin. In the 5 DIV *Rncr3*$^{-/-}$ retina, the number of cone cells was reduced in retina transfected with control shRNA (shControl), whereas the number of cone cells was significantly increased in retina transfected with *shLhx2* compared with the control ($P < 0.01$; **Fig. 8a–e**). The number of cone cells in *shLhx2*-infected wild-type retina was unaltered (**Fig. 8a,c**), suggesting that the *Lhx2* knockdown rescue phenotype is not a result of an off-target effect. In addition, we forced the expression of shLhx2 in primary cultured hippocampal neurons to determine whether downregulation of *Lhx2* can rescue *Rncr3*$^{-/-}$ dentate gyrus neuron axonal elongation (**Fig. 8f–j**). The average dentate granular axon length in the neurons in the top 25$^{th}$ percentile of the population (determined by axon length) was significantly increased in shControl-transfected *Rncr3*$^{-/-}$ dentate gyrus neurons ($P < 0.01$; **Fig. 8g**). The elongated *Rncr3*$^{-/-}$ dentate gyrus axon phenotype was restored to the wild-type level by transfection of *shLhx2* (**Fig. 8i,j**). These results suggest that *Lhx2* is a primary target gene of miR-124a and is responsible for the *Rncr3*$^{-/-}$ phenotypes, including both the reduction of retinal cone cell numbers and mossy fiber elongation of the dentate gyrus.

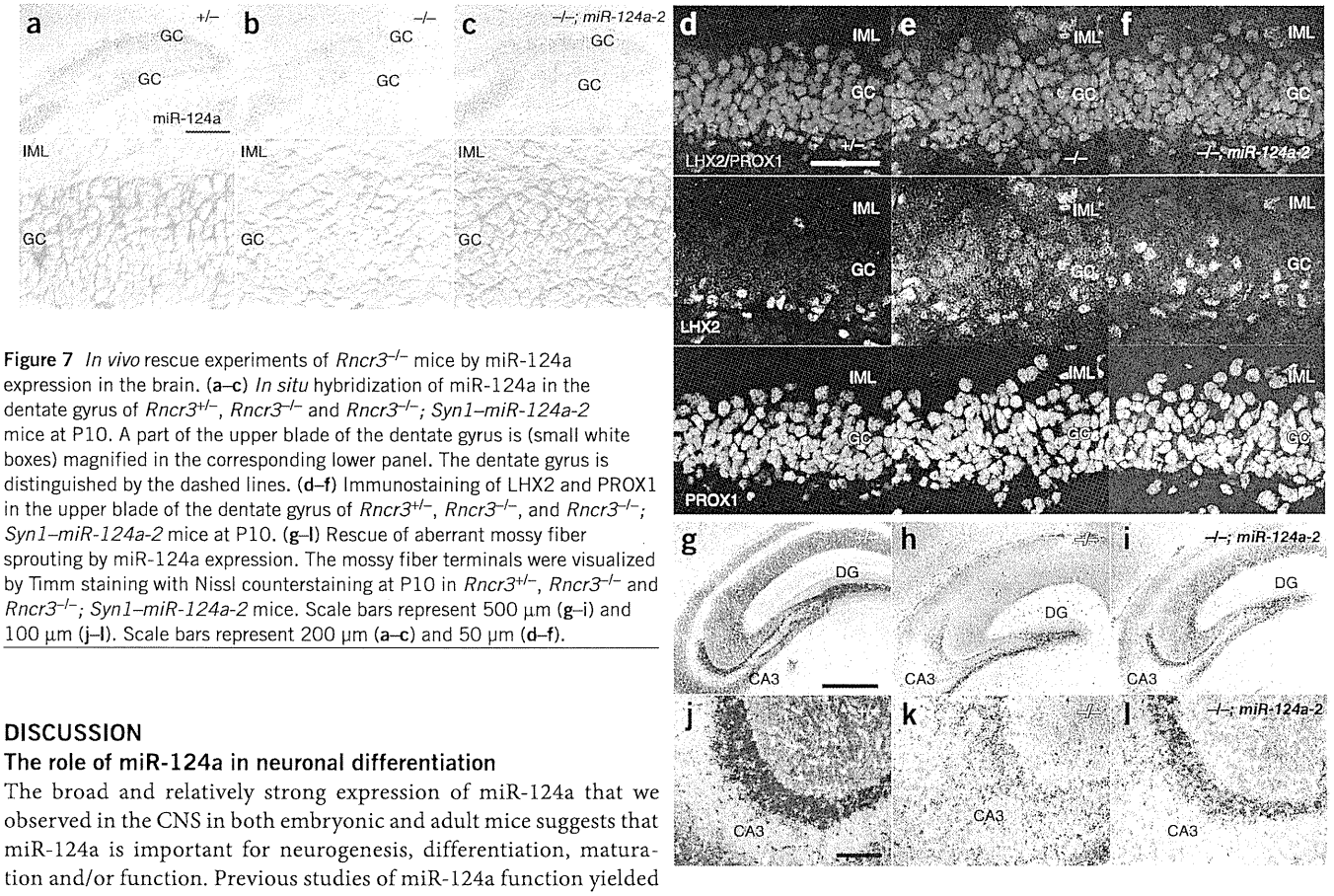


**Figure 7** *In vivo* rescue experiments of *Rncr3*$^{-/-}$ mice by miR-124a expression in the brain. (**a–c**) *In situ* hybridization of miR-124a in the dentate gyrus of *Rncr3*$^{+/-}$, *Rncr3*$^{-/-}$ and *Rncr3*$^{-/-}$*; Syn1–miR-124a-2* mice at P10. A part of the upper blade of the dentate gyrus is (small white boxes) magnified in the corresponding lower panel. The dentate gyrus is distinguished by the dashed lines. (**d–f**) Immunostaining of LHX2 and PROX1 in the upper blade of the dentate gyrus of *Rncr3*$^{+/-}$, *Rncr3*$^{-/-}$, and *Rncr3*$^{-/-}$*; Syn1–miR-124a-2* mice at P10. (**g–l**) Rescue of aberrant mossy fiber sprouting by miR-124a expression. The mossy fiber terminals were visualized by Timm staining with Nissl counterstaining at P10 in *Rncr3*$^{+/-}$, *Rncr3*$^{-/-}$ and *Rncr3*$^{-/-}$*; Syn1–miR-124a-2* mice. Scale bars represent 500 μm (**g–i**) and 100 μm (**j–l**). Scale bars represent 200 μm (**a–c**) and 50 μm (**d–f**).

## DISCUSSION

### The role of miR-124a in neuronal differentiation

The broad and relatively strong expression of miR-124a that we observed in the CNS in both embryonic and adult mice suggests that miR-124a is important for neurogenesis, differentiation, maturation and/or function. Previous studies of miR-124a function yielded inconsistent results. A previous study found that miR-124a did not act as a determinant of neuronal generation through both knockdown and overexpression experiments of miR-124a in the developing chick neural tube[7]. In contrast, another study found that miR-124a is required for neuronal determination in the developing chick neural tube[4]. Studies using *Dicer* conditional knockout mice have shown that miRNA is not necessary for neuronal determination[8,9]. In *Xenopus*, a knockdown experiment by micro-injection of locked nucleic acid (LNA)–modified anti–miR-124a oligonucleotides into the eight-cell stage revealed no obvious effect[27]. We observed normal neurogenesis in the developing photoreceptor layer and the dentate gyrus in *Rncr3*$^{-/-}$ mice in which miR-124a expression is mostly eliminated. These results are consistent with previous reports that miR-124a is expressed in the Ki67-negative postmitotic cells and regulated by the REST complex[6,28], suggesting that miR-124a functions in neuronal maturation and maintenance, rather than neuronal determination (**Supplementary Fig. 12**). It will be important to examine the role of miR-124a in neuronal determination and maturation in the future,

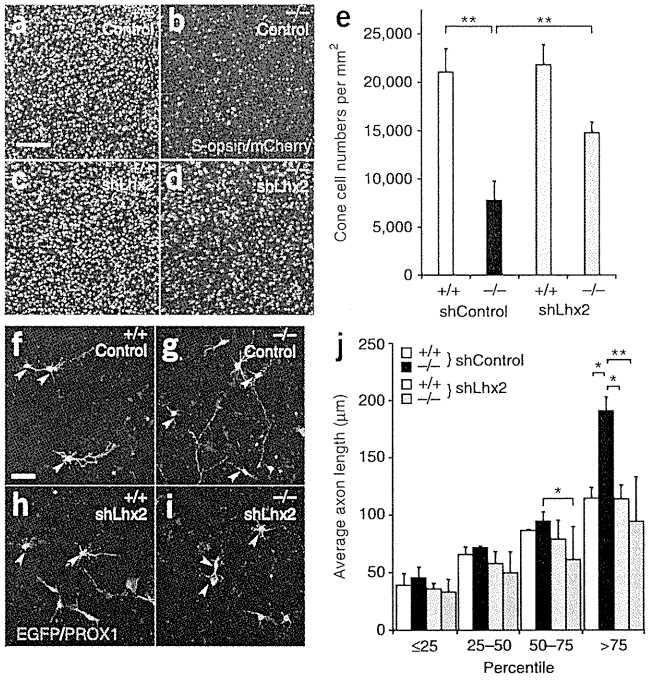


**Figure 8** Rescue of *Rncr3*$^{-/-}$ mice by pre-miR-124a-2 expression. (**a–e**) Flat-mount immunostaining of S-opsin in the 5 DIV cultured retina. P0 wild-type (**a**,**c**) and *Rncr3*$^{-/-}$ retinas (**b**,**d**) were dissected and transfected with *U6* promoter–driven *shControl* (**a**,**b**) or *shLhx2* (**c**,**d**) with bicistronic expression of *CMV-mCherry* using AAV5 (**a–d**). Scale bar represents 50 μm. We counted the numbers of S-opsin–positive cone cell (**$P < 0.01$, **e**). Error bars represent s.d. from the means of $n = 4$. (**f–j**) Axon length of dentate granule cells after 70 h culture. P0 hippocampus of wild-type and *Rncr3*$^{-/-}$ mice were isolated and dissociated, then transfected with a *pBAsi-shControl* or *pBAsi-shLhx2-3* plasmid together with a *pCAG-egfp* plasmid. After immunostaining for PROX1 and EGFP, confocal fluorescence images were obtained. Scale bar represents 50 μm (**f–i**). The average axon length were calculated in 0–25th, 25–50th, 50–75th and 75–100th percentile groups (*$P < 0.05$ and **$P < 0.01$, **j**). Error bars represent s.d. from the means of $n = 3$. A total of 243 neurons were measured.

and analysis of pre-miR-124a-1 and pre-miR-124a-2 double knockout or miR-124a-1, miR-124a-2 and miR-124a-3 triple knockout mice will be necessary to draw a definitive conclusion.

Although the number of cone cells was significantly reduced in *Rncr3*$^{-/-}$ mice ($P < 0.001$), rod photoreceptor cells did not seem to be significantly affected ($P > 0.65$; **Fig. 3c,d** and **Supplementary Fig. 4a**). When we expressed a pre-miR-124a-2 transgene in the developing photoreceptors of *Rncr3*$^{-/-}$ mice, the number of cone cells was increased (**Fig. 6d–i**), suggesting that rod cells and other retinal neurons compensate for miR-124a loss with pre-miR-124a-2. Previous studies of the *Dicer* conditional knockout mouse in the retina suggested that photoreceptor differentiation at late developmental stages requires miRNAs[9] and that, of the retinal cell types, photoreceptors are the most sensitive to an imbalance of miRNAs[29]. Our results suggest that miR-124a is one of the main miRNAs functioning in photoreceptor cell maturation.

### *In vivo* miR-124a target mRNAs

Several groups identified target mRNAs of miR-124a in the CNS using translation assay and *in vivo* knockdown analysis. It was recently suggested that CREB1 and *Actl6a* (*BAF53a*) are miR-124a target mRNAs in *Aplysia* and mouse, respectively[30,31]. *Sox9* was also reported to be a miR-124a target in SVZ adult neurogenesis[6]. *Ptbp1* and *Ctdsp1* were reported to be targets of miR-124a and are involved in neuronal gene regulation in cultured cells[4,5]. The pairing mechanism between miRNA and target mRNA is well established as a Watson-Crick pairing known as the miRNA seed match (especially nucleotides 2–7)[32–34]. Furthermore, it was recently found that guanidine:uridine wobble base-pairing between miRNA seed region and mRNA interferes with targeting activity[35]. Taking advantage of recently updated database information, we re-examined reported miR-124a targets using TargetScan 5.1 and found *Lhx2*, a miR-124a target mRNA candidate in both humans and mice, as well as *Ptbp1*, and *Ctdsp1*. Although *Lhx2* or *Neurod1* were predicted to be miR-124a target mRNAs by a miR-124a overexpression experiment in *Xenopus*[27,36], precursor miRNA overexpression may mistakenly produce a phenotype as a result of an effect on the miRNA synthesis mechanism or off-target effects. In fact, we did not detect a significant change in NEUROD1 protein and *Otx2* transcript expression ($P > 0.79$; **Fig. 2i–l** and **Supplementary Fig. 5g,k,n**), both of which were affected by pre-miR-124a overexpression in the *Xenopus* study[27,36]. Here, we found that *Lhx2* is a target of miR-124a in retinal cones and in the dentate gyrus in *Rncr3*$^{-/-}$ mice (**Fig. 5** and **Supplementary Fig. 8a–d**). Furthermore, LHX2 protein localization did not overlap with *Lhx2* mRNA distribution in regions in which *Rncr3* was expressed (**Supplementary Fig. 8f–o**). These observations suggest that LHX2 protein expression is affected by miR-124a by translational inhibition. We also performed both a luciferase assay and qPCR of luciferase mRNA (**Supplementary Fig. 8c,d**). Notably, although the luciferase activity of the construct containing a miR-124a target sequence in its 3′ UTR was decreased by miR-124a expression, the level of luciferase mRNA was unchanged. Our *Lhx2* overexpression assay revealed that cell death was increased in the developing retina, suggesting that inhibition of *Lhx2* translation by miR-124a is one of the essential mechanisms for down-regulating *Lhx2* in the normal development of retinal cells (**Supplementary Fig. 12**).

*Lhx2* functions as a selector gene for forebrain and eye development[37]. *Lhx2*-expressing normal dorsal telencephalon cells show a marked tendency to form aggregation clusters[24], implying that LHX2 contributes to the regionalization of the cortical hem (LHX2 negative) and the non–cortical hem hippocampal region (LHX2 positive)[24]. In the *Rncr3*$^{-/-}$ brain, elevation of LHX2 protein levels may lead to a higher density of dentate neurons by promoting cell aggregation (**Fig. 5i,j,l**). Furthermore, we observed aberrant sprouting of dentate gyrus axons, mossy fibers, into the CA3 region in the *Rncr3*$^{-/-}$ brain (**Fig. 4e–h**), and found that the LHX2 level affects axonal outgrowth in primary cultured hippocampal dentate neurons (**Figs. 5m–u** and **8f–j**). It was recently shown that commissural neurons, which express LHX2 protein, extend their axons, but fail to cross the midline in *Lhx2* and *Lhx9* double knockout mice, suggesting that *Lhx2*-defective commissural neurons do not respond well to guidance cues[38]. In contrast, in the CA3 region of the *Rncr3*$^{-/-}$ hippocampus, we hypothesize that dentate gyrus granule cells may have an axon elongation capability and may over-respond to guidance cues, resulting in the mis-sprouting of granule cells to the CA3 region. Although elevated LHX2 may induce the aberrant axonal elongation phenotype, it should be noted that increased cell density and aberrant sprouting of dentate neurons in the hippocampus have been observed in seizure-induced rats[39]. Thus, understanding the precise mechanism that underlies these phenotypes awaits future study. Taken together, our findings suggest that LHX2 protein level regulation by miR-124a is critical for dentate gyrus maturation and survival (**Supplementary Fig. 12**).

### Implication of miR-124a in human diseases

In humans, pre-miR-124a-1 is located on chromosome 8p23.1. Notably, chromosomal duplication, deletion or mutation of the 8p23.1 region have been reported to be involved in cerebral development and neuropsychiatric disorders, including autism, bipolar disorder, schizophrenia, learning difficulties, epilepsy and microcephaly[2,40,41]. In individuals with temporal lobe epilepsy and model animals, aberrantly sprouting mossy fibers are often observed[42]. However, the molecular mechanisms remain unknown. We found that a substantial reduction or loss of mature miR-124a (by 60–80%) or loss of miR-124a-1 resulted in a small brain, neuronal dysfunction and aberrant axonal sprouting in the hippocampus (**Fig. 4**), suggesting that dis-regulation of the miR-124a expression level is involved in developmental neuropsychiatric disorders and temporal lobe epilepsy in humans with chromosome 8p abnormalities.

A recent study of FMRP, a protein that is involved in a fragile X syndrome and a RISC component interacting with Argonaute, suggested that miR-124a interacts with the FMRP protein, which is present at synapses[43,44]. It was recently reported that miR-124a is bound and regulated by dFMR1, a FMRP protein in *Drosophila*[45]. Another study found that miR-124a is present in sensory-motor synapses and is involved in synaptic plasticity through CREB in *Aplysia*[30]. Thus, it was suggested that miR-124a is important for synaptic function. In contrast, it should be noted that another study using rat hippocampal neurons found that mature miR-124a is not enriched in synaptosomes[46]. Further analysis will be needed to fully understand the role of miR-124a in synaptic functions.

There are three pre-miR-124a loci (pre-miR-124a-1, pre-miR-124a-2 and pre-miR-124a-3) in the mouse and human genomes. Our findings strongly suggest that *Rncr3* is the primary source of miR-124a. Production and analysis of miR-124a double and/or triple knockout mice, if the mutations are not lethal, will further clarify *in vivo* miR-124a function and target mRNAs in other parts of the CNS.

## METHODS

Methods and any associated references are available in the online version of the paper at http://www.nature.com/natureneuroscience/.

*Note: Supplementary information is available on the Nature Neuroscience website.*

ACKNOWLEDGMENTS

We thank T. Maniatis for *RIPmiR-124a-2*, M. Kilimann for *Synapsin 1* promoter, Y. Omori, K. Terada, M. Ueno, N. Nagata, K. Aritake, Y. Oishi, T. Hamasaki, and H. Abe for critical comments and technical advice, and A. Tani, M. Kadowaki, Y. Kawakami, A. Ishimaru, H. Tsujii, T. Saioka, K. Sone, H. Abe, and S. Kennedy for technical assistance. This work was supported by Japan Science and Technology Agency (JST), Core Research for Evolutional Science and Technology (CREST), Grant-in-Aid for Scientific Research (B), Grant-in-Aid for Young Scientists (B), a Grant for Molecular Brain Science from the Ministry of Education, Culture, Sports, Science and Technology, the Takeda Science Foundation, the Uehara Memorial Foundation, the Mochida Memorial Foundation, and the Naito Foundation.

AUTHOR CONTRIBUTIONS

R.S. and T.F. designed the project. R.S., C.K., S.W., S.I. and T.F carried out the molecular and *in situ* hybridization experiments. R.S. and A.O. performed *in vivo* electroporation, virus infection and knockdown experiments in retinal and hippocampal neurons, and immunohistochemistry. S.U., T.K., M.K. and R.S. carried out the ERG experiments. R.S., Y.M. and T.F. produced the knockout and transgenic mice. R.S., R. Muramatsu and T.Y. carried out hippocampal tissue experiments. R.S., R. Matsui and D.W. produced lentivirus. R.S., Y.C. and Y.U. produced adeno-associated virus. R.S. and T.F. wrote the manuscript. T.F. supervised the project.

COMPETING FINANCIAL INTERESTS

The authors declare no competing financial interests.

Published online at http://www.nature.com/natureneuroscience/.
Reprints and permissions information is available online at http://www.nature.com/reprints/index.html.



1. Lagos-Quintana, M. *et al.* Identification of tissue-specific microRNAs from mouse. *Curr. Biol.* **12**, 735–739 (2002).
2. Tabarés-Seisdedos, R. & Rubenstein, J.L. Chromosome 8p as a potential hub for developmental neuropsychiatric disorders: implications for schizophrenia, autism and cancer. *Mol. Psychiatry* **14**, 563–589 (2009).
3. Lim, L.P. *et al.* Microarray analysis shows that some microRNAs downregulate large numbers of target mRNAs. *Nature* **433**, 769–773 (2005).
4. Visvanathan, J., Lee, S., Lee, B., Lee, J.W. & Lee, S.K. The microRNA miR-124 antagonizes the anti-neural REST/SCP1 pathway during embryonic CNS development. *Genes Dev.* **21**, 744–749 (2007).
5. Makeyev, E.V., Zhang, J., Carrasco, M.A. & Maniatis, T. The microRNA miR-124 promotes neuronal differentiation by triggering brain-specific alternative pre-mRNA splicing. *Mol. Cell* **27**, 435–448 (2007).
6. Cheng, L.C., Pastrana, E., Tavazoie, M. & Doetsch, F. miR-124 regulates adult neurogenesis in the subventricular zone stem cell niche. *Nat. Neurosci.* **12**, 399–408 (2009).
7. Cao, X., Pfaff, S.L. & Gage, F.H. A functional study of miR-124 in the developing neural tube. *Genes Dev.* **21**, 531–536 (2007).
8. De Pietri Tonelli, D. *et al.* miRNAs are essential for survival and differentiation of newborn neurons but not for expansion of neural progenitors during early neurogenesis in the mouse embryonic neocortex. *Development* **135**, 3911–3921 (2008).
9. Georgi, S.A. & Reh, T.A. Dicer is required for the transition from early to late progenitor state in the developing mouse retina. *J. Neurosci.* **30**, 4048–4061 (2010).
10. Koike, C. *et al.* TRPM1 is a component of the retinal ON bipolar cell transduction channel in the mGluR6 cascade. *Proc. Natl. Acad. Sci. USA* **107**, 332–337 (2010).
11. Blackshaw, S. *et al.* Genomic analysis of mouse retinal development. *PLoS Biol.* **2**, e247 (2004).
12. He, S. *et al.* MicroRNA-encoding long non-coding RNAs. *BMC Genomics* **9**, 236 (2008).
13. Hackler, L., Wan, J., Swaroop, A., Qian, J. & Zack, D.J. MicroRNA profile of the developing mouse retina. *Invest. Ophthalmol. Vis. Sci.* **51**, 1823–1831 (2010).
14. Ohsawa, R. & Kageyama, R. Regulation of retinal cell fate specification by multiple transcription factors. *Brain Res.* **1192**, 90–98 (2008).
15. Cepko, C.L., Austin, C.P., Yang, X., Alexiades, M. & Ezzeddine, D. Cell fate determination in the vertebrate retina. *Proc. Natl. Acad. Sci. USA* **93**, 589–595 (1996).
16. Ng, L. *et al.* A thyroid hormone receptor that is required for the development of green cone photoreceptors. *Nat. Genet.* **27**, 94–98 (2001).
17. Furukawa, T., Morrow, E.M. & Cepko, C.L. Crx, a novel otx-like homeobox gene, shows photoreceptor-specific expression and regulates photoreceptor differentiation. *Cell* **91**, 531–541 (1997).
18. Chen, S. *et al.* Crx, a novel Otx-like paired-homeodomain protein, binds to and transactivates photoreceptor cell-specific genes. *Neuron* **19**, 1017–1030 (1997).
19. Nishida, A. *et al.* Otx2 homeobox gene controls retinal photoreceptor cell fate and pineal gland development. *Nat. Neurosci.* **6**, 1255–1263 (2003).
20. Silber, J. *et al.* miR-124 and miR-137 inhibit proliferation of glioblastoma multiforme cells and induce differentiation of brain tumor stem cells. *BMC Med.* **6**, 14 (2008).
21. Côté, F., Collard, J.F. & Julien, J.P. Progressive neuronopathy in transgenic mice expressing the human neurofilament heavy gene: a mouse model of amyotrophic lateral sclerosis. *Cell* **73**, 35–46 (1993).
22. Okazaki, M.M., Evenson, D.A. & Nadler, J.V. Hippocampal mossy fiber sprouting and synapse formation after status epilepticus in rats: visualization after retrograde transport of biocytin. *J. Comp. Neurol.* **352**, 515–534 (1995).
23. Chow, R.L. & Lang, R.A. Early eye development in vertebrates. *Annu. Rev. Cell Dev. Biol.* **17**, 255–296 (2001).
24. Mangale, V.S. *et al.* Lhx2 selector activity specifies cortical identity and suppresses hippocampal organizer fate. *Science* **319**, 304–309 (2008).
25. Furukawa, A., Koike, C., Lippincott, P., Cepko, C.L. & Furukawa, T. The mouse Crx 5′-upstream transgene sequence directs cell-specific and developmentally regulated expression in retinal photoreceptor cells. *J. Neurosci.* **22**, 1640–1647 (2002).
26. Hoesche, C., Sauerwald, A., Veh, R.W., Krippl, B. & Kilimann, M.W. The 5′-flanking region of the rat synapsin I gene directs neuron-specific and developmentally regulated reporter gene expression in transgenic mice. *J. Biol. Chem.* **268**, 26494–26502 (1993).
27. Qiu, R. *et al.* The role of miR-124a in early development of the *Xenopus* eye. *Mech. Dev.* **126**, 804–816 (2009).
28. Conaco, C., Otto, S., Han, J.J. & Mandel, G. Reciprocal actions of REST and a microRNA promote neuronal identity. *Proc. Natl. Acad. Sci. USA* **103**, 2422–2427 (2006).
29. Damiani, D. *et al.* Dicer inactivation leads to progressive functional and structural degeneration of the mouse retina. *J. Neurosci.* **28**, 4878–4887 (2008).
30. Rajasethupathy, P. *et al.* Characterization of small RNAs in aplysia reveals a role for miR-124 in constraining synaptic plasticity through CREB. *Neuron* **63**, 803–817 (2009).
31. Yoo, A.S., Staahl, B.T., Chen, L. & Crabtree, G.R. MicroRNA-mediated switching of chromatin-remodeling complexes in neural development. *Nature* **460**, 642–646 (2009).
32. Friedman, R.C., Farh, K.K., Burge, C.B. & Bartel, D.P. Most mammalian mRNAs are conserved targets of microRNAs. *Genome Res.* **19**, 92–105 (2009).
33. Lewis, B.P., Burge, C.B. & Bartel, D.P. Conserved seed pairing, often flanked by adenosines, indicates that thousands of human genes are microRNA targets. *Cell* **120**, 15–20 (2005).
34. Lewis, B.P., Shih, I.H., Jones-Rhoades, M.W., Bartel, D.P. & Burge, C.B. Prediction of mammalian microRNA targets. *Cell* **115**, 787–798 (2003).
35. Doench, J.G. & Sharp, P.A. Specificity of microRNA target selection in translational repression. *Genes Dev.* **18**, 504–511 (2004).
36. Liu, K. *et al.* MiR-124 regulates early neurogenesis in the optic vesicle and forebrain, targeting NeuroD1. *Nucleic Acids Res.* **39**, 2869–2879 (2011).
37. Porter, F.D. *et al.* Lhx2, a LIM homeobox gene, is required for eye, forebrain and definitive erythrocyte development. *Development* **124**, 2935–2944 (1997).
38. Wilson, S.I., Shafer, B., Lee, K.J. & Dodd, J. A molecular program for contralateral trajectory: Rig-1 control by LIM homeodomain transcription factors. *Neuron* **59**, 413–424 (2008).
39. Holmes, G.L., Sarkisian, M., Ben-Ari, Y. & Chevassus-Au-Louis, N. Mossy fiber sprouting after recurrent seizures during early development in rats. *J. Comp. Neurol.* **404**, 537–553 (1999).
40. Baulac, S. *et al.* A novel locus for generalized epilepsy with febrile seizures plus in French families. *Arch. Neurol.* **65**, 943–951 (2008).
41. Glancy, M. *et al.* Transmitted duplication of 8p23.1–8p23.2 associated with speech delay, autism and learning difficulties. *Eur. J. Hum. Genet.* **17**, 37–43 (2009).
42. Koyama, R. & Ikegaya, Y. Mossy fiber sprouting as a potential therapeutic target for epilepsy. *Curr. Neurovasc. Res.* **1**, 3–10 (2004).
43. Weiler, I.J. *et al.* Fragile X mental retardation protein is translated near synapses in response to neurotransmitter activation. *Proc. Natl. Acad. Sci. USA* **94**, 5395–5400 (1997).
44. Edbauer, D. *et al.* Regulation of synaptic structure and function by FMRP-associated microRNAs miR-125b and miR-132. *Neuron* **65**, 373–384 (2010).
45. Xu, X.L., Li, Y., Wang, F. & Gao, F.B. The steady-state level of the nervous system–specific microRNA-124a is regulated by dFMR1 in *Drosophila*. *J. Neurosci.* **28**, 11883–11889 (2008).
46. Siegel, G. *et al.* A functional screen implicates microRNA-138-dependent regulation of the depalmitoylation enzyme APT1 in dendritic spine morphogenesis. *Nat. Cell Biol.* **11**, 705–716 (2009).

## ONLINE METHODS

**Animal care.** All procedures conformed to the ARVO Statement for the Use of Animals in Ophthalmic and Vision Research and were approved by the Institutional Safety Committee on Recombinant DNA Experiments and the Animal Research Committee of Osaka Bioscience Institute. Mice were housed in a temperature-controlled room at 22 °C with a 12 h light/dark cycle. Fresh water and rodent diet were available at all times.

**Generation of *Rncr3*$^{-/-}$ mice.** We obtained *Rncr3* genomic clones from a screen of the 129/SvEv mouse genomic DNA library (Stratagene). We subcloned a 6.5-kb SalI-EcoRI fragment and a 4.4-kb SalI-SalI fragment from *Rncr3* genomic clones into a modified *pPNT* vector, and transfected the linearized targeting construct into the TC1 embryonic stem cell line. Genomic DNA from the liver was digested with BamHI or EcoRV, and hybridized with 5′ and 3′ probes, respectively.

**Northern blot analysis.** Northern blot analysis was performed as described previously[47]. An approximately 2.2-kb fragment (the BglII-BglII fragment) of mouse *Rncr3* cDNA (GenBank #BC096449) was used to synthesize the DNA probe.

**PAGE northern for miR-124a.** Total RNAs from mouse tissues were isolated by Trizol (Invitrogen). We denatured 20 μm of total RNAs in 5 mM EDTA containing formamide at 80 °C for 5 min, then separated them on 15% denaturing (7 M urea) polyacrylamide gels. RNAs were transferred to a nylon membrane (Pall Corporation Biodyne) at a constant current (3.3 mA cm$^{-2}$) for 35 min. The filter was baked for 1 h at 80 °C. LNA-modified anti-miR-124a (EXIQON, 20 pmol) was end-labeled with γ-$^{32}$P-ATP (3,000 Ci mmol$^{-1}$, Muromachi Yakuhin) using T4 polynucleotide kinase (Takara) and purified on spin columns (GE Healthcare Micro SpinTM G-25). The nylon filters were hybridized with the labeled probe in salmon sperm-containing hybridization solution (120 mM sodium phosphate (pH 7.2), 250 mM sodium chloride, 7% SDS (wt/vol) and 50% formamide (vol/vol) at 43 °C overnight, and washed twice with 0.1% SDS containing 2× SSC at 25 °C for 5 min. The filters were then exposed to X-ray film.

***In situ* hybridization.** *In situ* hybridization was performed as described previously[47]. Digoxigenin-labeled riboprobes were synthesized by T7, SP6, or T3 RNA polymerase using the *Rncr3* (same as the 3′ probe region in northern blots), *pri-miR-124a-2* (**Supplementary Table 1**), *Lhx2* (ref. 48, **Supplementary Table 1**), *Ngn2* (an EcoRI-*Xba*I fragment of cDNA AK143190), *Crx* or *Otx2* (ref. 19) cDNA as a template in the presence of 11-digoxigenin UTPs (Roche). For miR-124a detection, we used anti-miR-124a modified with a digoxigenin-labeled LNA probe (EXIQON).

**Immunostaining.** For immunohistochemistry, 14-μm retina and brain sections were washed twice in phosphate-buffered saline (PBS), and permeabilized with 0.1% Triton X-100 (wt/vol) in PBS, then incubated with PBS containing 4% donkey serum (vol/vol) for 1 h to block samples. The samples were incubated with a primary antibody (**Supplementary Table 2**) at 4 °C overnight. After PBS-washing, these samples were incubated with secondary antibodies at 25 °C for 1 h.

For whole-mount immunostaining of the retina, each retina was gently peeled off from the sclera, rinsed in PBS and fixed with 4% paraformaldehyde (wt/vol) in PBS for 2 h. The retinas were permeabilized by incubation in 0.1% Triton X-100 in PBS for 30 min. After washing in PBS, samples were blocked with 4% donkey serum and 0.02% Triton X-100 in PBS for 3 h. The retinas were then immunostained with primary antibodies to M-opsin and S-opsin (**Supplementary Table 2**) at 4 °C overnight. Reactions with secondary antibodies were performed overnight at 4 °C.

**Western blot analysis.** Western blot analysis was performed as described previously[47]. The membrane was incubated with mouse antibody to Flag (1:5,000, Sigma) or goat antibody to LHX2 (3:500; Abcam). The membrane was then incubated with a horseradish peroxidase-conjugated donkey antibody to mouse IgG (1:10,000, Jackson) or rabbit antibody to goat IgG (1:10,000, Zymed). For secondary immunoreaction, the PVDF membrane was incubated with WB Stripping Solution (Nacalai Tesque) to remove antibodies, and blocked again with 5% skim milk (wt/vol) in TBS. Further immunoblots were performed using rat antibody to GFP (1:2,000, Nacalai Tesque) or mouse antibody to β-actin (ACTB, 1:5,000, Sigma). The signals were measured using ImageJ (US National Institutes of Health).

**ERG.** Electroretinographic recordings were performed as described in detail[47]. In brief, ERGs were picked-up with a gold-wire loop electrode placed on the cornea. The mice were placed in a Ganzfeld bowl and stimulated with four levels of stroboscopic stimuli ranging from −5.0 to 1.0 log cd s m$^{-2}$ to elicit scotopic ERGs, and four levels of stimuli ranging from −0.5 to 1.0 log cd s m$^{-2}$ for the photopic ERGs. The photopic ERGs were recorded on a rod-suppressing white background of 1.3 log cd m$^{-2}$.

**Plasmid constructs.** The *Lhx2* cDNA fragment was amplified by PCR (**Supplementary Table 1**) using PrimeStar (Takara), and cloned into the *pGEM-TEasy* vector (Promega). *Lhx2* 3′ UTR-containing fragments were also amplified and cloned into *pGEM-TEasy*. Mutations in the seed match region were introduced by PCR primers (**Supplementary Table 1**). The fragments of *Lhx2* cDNA and *Lhx2* 3′ UTR were ligated into the *pCAGGS* vector. To perform the luciferase assay, we constructed a miR-124a expression plasmid. Pre-miR-124-1, pre-miR-124-2 and pre-miR-124-3 were amplified by PCR (**Supplementary Table 1**) using ExTaq polymerase (Takara), and each PCR-amplified fragment was cloned into *pCRII* plasmids (Invitrogen). After verifying the sequence, we subcloned them into *pBAsi-mU6* (Takara). The *Lhx2* 3′ UTR were ligated into *pmirGLO* (Promega) to generate *pmirGLO-Lhx2-Nat* and *pmirGLO-Lhx2-Mut*. For *Lhx2* knockdown, *pBAsi-mU6* was used for DNA vector-based shRNA synthesis. Three target sequences, shLhx2-1, shLhx2-2 and shLhx2-3 (**Supplementary Table 1**), were selected from different positions in the mouse *Lhx2* open reading frame and subcloned into the *pBAsi-mU6* vector. The inhibition abilities of shLhx2-1, shLhx2-2 and shLhx2-3 were tested by western blot analysis using cultured cells (**Supplementary Fig. 11a,b**). The strongest inhibitor of Lhx2, shLhx2-3, was used.

**Generation of miR-124a-2 transgenic mice.** The *pCrx2k-Cre* plasmid[19] was digested with XhoI and BamHI to remove the *Cre* gene (*pCrx2k*). *RIP-miR-124a-2* (a gift from T. Maniatis, Harvard University)[5] is a pre-miR-124a-2 expression vector that encodes pre-miR-124a-2 in an intron of the *Ds-Red* gene. We digested *RIP-miR-124a-2* and ligated it into the *pCrx2k* plasmid (*pCrx2k-Ds-Red-124a-2*; **Supplementary Fig. 9a**). To construct a transgene vector of miR-124a-2 to rescue the hippocampal phenotype, we ligated the *pUC18-4.3Syn-CAT* plasmid (a gift from M. Kilimann, Ruhr-Universität Bochum)[26] containing a rat 4.3-kb *Syn1* promoter into Ds-red-124a-2 (*pSyn14.3k-Ds-Red-124a-2*; **Supplementary Fig. 10a**). The purified construct was injected into the pronuclei of fertilized one-cell eggs of B6C3F1 mice (Oriental Bio Service) followed by implantation into pseudopregnant foster mothers (ICR mice, Japan SLC).

**Luciferase assay.** We transfected 0.5 μg of the reporter plasmid DNA (*pmirGLO*, *pmirGLO-Lhx2-3′ UTR-Nat* or *pmirGLO-Lhx2-3′ UTR-Mut*) and 2 μg of miR-124a expression vector DNA (*pBAsi-mU6*, *pBAsi-mU6-pre-miR-124a-1*, *pBAsi-mU6-pre-miR-124a-2* or *pBAsi-mU6-pre-miR-124a-3*) per well into HEK 293T cells in a 6-well plate using the calcium phosphate method. After transfection, the cells were incubated for 48 h and lysed with Reporter Lysis Buffer (Promega). P0 hippocampal cells (approximately 2 × 10$^5$) were transfected with *pmirGLO-Lhx2-3′ UTR-Nat*, or *pBAsi-mU6-pre-miR-124a-1-Mut* (250 ng each) by electroporation (Amaxa Nucleofector). After transfection, the cells were incubated for 72 h, washed with PBS, and lysed with Reporter Lysis Buffer. The lysates were used for luciferase assays. Luciferase activity was measured with the Dual-Glo Luciferase Assay System (Promega) according to the manufacturer's protocol using a Wallac 1420 Multilabel Counter (Wallac). Firefly luciferase activities were determined by three independent transfections and normalized by comparison with the Renilla luciferase activities of the internal control.

***In vivo* electroporation.** *In vivo* electroporation was performed on the P0 mouse retina as described previously[47]. The *pCAGGS*, *pCAGGS-Lhx2-Nat* or *pCAGGS-Lhx2-Mut* vectors were co-electroporated with the *pCAGGS-EGFP* vector. We used *pCAGGS* vector concentrations of 0, 2 and 3 μg μl$^{-1}$, *pCAGGS-Lhx2* (native or mutated) concentrations of 4, 2 and 1 μg μl$^{-1}$, and a *pCAGGS-EGFP* concentration of 1 μg μl$^{-1}$ to make a 5 μg μl$^{-1}$ DNA solution mix. The electroporated retinas were harvested at P4.

**TUNEL assay.** Fresh frozen retinas were sectioned to a thickness of 14 μm and fixed with 4% paraformaldehyde in PBS for 1 min. The TUNEL assay was performed according to the manufacturer's protocols.

**RT-PCR and qPCR analysis.** Total RNA was extracted Trizol reagent (Invitrogen), and reverse transcribed into cDNA using SuperScript II reverse transcriptase (Invitrogen) with random hexamers. Quantitative PCR was performed using a SYBR GreenER qPCR SuperMix Universal (Invitrogen). Nucleotide sequences of primers are shown in **Supplementary Table 1**. To detect mature miR-124a, we isolated total RNA using the miRNeasy Mini Kit (Qiagen), and reverse transcribed using the miScript Reverse Transcription Kit (Qiagen). Real-time qRT-PCR was performed using the miScript SYBR Green PCR kit with miScript Universal primer and the miScript Primer assay (Qiagen). For the pri-miR-124a expression assay, total RNA isolated using the miRNeasy Mini Kit was reverse transcribed to cDNA using the TaqMan reverse transcription reagent kit and following the manufacturer's protocol (Applied Biosystems). Real-time qRT-PCR was performed using TaqMan Universal PCR Master Mix and specific TaqMan Pri-miRNA Assays for *Mus musculus* miR-124-1, miR-124-2 and miR-124-3 (Applied Biosystems).

**Behavior test.** *Rncr3*$^{-/-}$ and wild-type mice (4–5 months old) were suspended by their tails for 3 min, and clasping duration time was measured.

**Timm staining and Nissl staining.** Coronal sections, 14 μm thick, from P10 frozen mouse brains were stained by the neo-Timm's method[49]. After washing in de-ionized water, sections were counterstained by 0.1%(w/v) cresyl violet (wt/vol) for 5 min, washed in 100% ethanol, and incubated in xylene. Slides were coverslipped with Permount (Fisher Scientific).

**Axon outgrowth assay.** Neurons from P0 mouse hippocampus were dissociated using Nerve Cell Dissociation Medium (SUMILON) according to the manufacturer's protocol. The hippocampal cells (the approximate numbers are $4 \times 10^5$) were transfected with *pCAGGS*, *pCAGGS-Lhx2-Nat* or *pCAGGS-Lhx2-Mut* (250 ng each) together with the transfected cell marker plasmid, 125 ng of *pCAGGS-FGFP* by electroporation (Amaxa Nucleofector). Then, cells were cultured on 3.5-cm poly-D-lysine–coated dishes in Nerve-Cell Culture Medium (SUMILON). For Lhx2 knockdown experiments, hippocampal cells (the approximate numbers are $2 \times 10^5$) were transfected with *pBAsi-shControl*[50] or *pBAsi-shLhx2-3* (250 ng each), together with a transfected cell marker plasmid, *pCAGGS-FGFP*. At 72 h, the cells were fixed with 4% paraformaldehyde, 4% sucrose (wt/vol), and 0.02% Triton X-100 in PBS for 30 min, then washed with PBS. After blocking with 4% donkey serum in PBS, cells were incubated with primary antibodies to PROX1 and EGFP (**Supplementary Table 2**). Following PBS washes, Alexa 488–conjugated antibody to rat IgG and Cy3-conjugated antibody to rabbit IgG were used as secondary antibodies. Images of these cells were obtained using a confocal microscope LSM700 (Zeiss), and PROX1-positive axons (longest neurite) were measured using the LSM image browser (Zeiss).

**Hippocampal slice culture.** A P6 SD rat brain was dissected and sliced (300 μm thick). The hippocampal slices were placed onto membranes of Millicell-CM culture inserts (Millipore) and infected with *Camk2a* promoter–driven *Lhx2-IRES-mCherry* or *mock (control)-IRES-mCherry* expression lentivirus (approximately $10^{10}$ PFU ml$^{-1}$ titer) into three loci of the dentate molecular layer using a micromanipulator. Nutrition medium was composed of 25% heat-inactivated horse serum, 25% Hank's balanced salt solution, and 50% MEM. The medium was changed every 2 d. After 5 DIV, the cultured slice was fixed with 4% paraformaldehyde, 4% sucrose and 0.02% Triton X-100 in PBS for 3 h, then permeabilized with PBS, and 0.1% Triton X-100 for 30 min. The sliced section was further immunostained.

**Retinal explant culture and AAV infection.** The P0 eyes were enucleated, and the choroid, sclera and cornea were removed. The eyecups (retinas with lens and vitreous) were incubated with fresh DMEM/F12 media containing AAV5 (approximately $1 \times 10^{12}$ particles per ml titer), which bicistronically expresses *shControl* or *shLhx2* driven by the *U6* promoter and *mCherry* driven by the *CMV* promoter (*U6-shControl-CMV-mCherry* or *U6-shLhx2- CMV-mCherry*) for 1 h at 25 °C. The lens and vitreous were removed, and the retinas were explanted with the photoreceptor side up. After a 30-min incubation, 5 μl of AAV5 vector (approximately $1 \times 10^{12}$ particles) was dropped to cover the surface of the explants. The explants cultured for 5 d were immunostained with an antibody to S-opsin.

**Statistical analysis.** Statistical comparison of datasets were performed with Student's *t*-test. For multiple comparison, we performed one-way ANOVA with Tukey-Kramer test or Kruskal-Wallis non-parametric ANOVA with Steel-Dwass multiple comparison test. Complete statistical information is described in the **Supplementary Statistical Analysis**.


47. Sanuki, R., Omori, Y., Koike, C., Sato, S. & Furukawa, T. Panky, a novel photoreceptor-specific ankyrin repeat protein, is a transcriptional cofactor that suppresses CRX-regulated photoreceptor genes. *FEBS Lett.* **584**, 753–758 (2010).
48. Gray, P.A. *et al.* Mouse brain organization revealed through direct genome-scale TF expression analysis. *Science* **306**, 2255–2257 (2004).
49. Babb, T.L., Kupfer, W.R., Pretorius, J.K., Crandall, P.H. & Levesque, M.F. Synaptic reorganization by mossy fibers in human epileptic fascia dentata. *Neuroscience* **42**, 351–363 (1991).
50. Onishi, A. *et al.* Pias3-dependent SUMOylation directs rod photoreceptor development. *Neuron* **61**, 234–246 (2009).





doi:10.1038/nn.2897

# REBOUND OF MACULAR EDEMA AFTER INTRAVITREAL BEVACIZUMAB THERAPY IN EYES WITH MACULAR EDEMA SECONDARY TO BRANCH RETINAL VEIN OCCLUSION

SHUNSUKE YASUDA, MD, MINEO KONDO, MD, PHD, SHU KACHI, MD, PHD, YASUKI ITO, MD, PHD, TAKAYUKI TERUI, MD, SHINJI UENO, MD, PHD, HIROKO TERASAKI, MD, PHD

**Purpose:** To determine the incidence of rebound macular edema after intravitreal bevacizumab in eyes with macular edema secondary to branch retinal vein occlusion and to identify the pretreatment factors that were significantly associated with the rebound.

**Methods:** The changes in the foveal thickness after the intravitreal bevacizumab (1.25 mg/0.05 mL) were studied in 65 eyes of 65 patients with macular edema secondary to branch retinal vein occlusion. A rebound of macular edema was defined as a ≥110% increase in the foveal thickness or a foveal thickness ratio of ≥110% (foveal thickness at the recurrence/foveal thickness at the baseline × 100). Multivariate logistic regression analyses and subgroup analyses were performed to determine which pretreatment factors were associated with the rebound.

**Results:** Seven of 65 eyes (10.8%) showed a rebound (≥110% of baseline thickness). Subgroup analyses showed that a thinner pretreatment fovea and a shorter interval between symptom onset to the initiation of the intravitreal bevacizumab were significantly associated with a rebound of macular edema ($P < 0.01$). The interval from symptoms onset to the initiation of treatment was <8 weeks in all 7 eyes with a rebound macular edema.

**Conclusion:** These results suggest that a rebound of macular edema in eyes with branch retinal vein occlusion was more likely to occur when the intravitreal bevacizumab therapy is initiated before the macular edema reaches the maximum level. Rebound of macular edema may be effectively avoided by waiting at least 8 weeks after the onset of symptoms to begin the intravitreal bevacizumab.

**RETINA** 31:1075–1082, 2011

Macular edema is one of the most common complications and major cause of visual decrease in eyes with branch retinal vein occlusion (BRVO).[1–3] The Branch Vein Occlusion Study Group reported on the long-term visual prognosis of 35 untreated patients with macular edema after BRVO and a decrease of visual acuity to ≤20/40. They found that two thirds of these eyes had a visual acuity <20/40 after 3 years.[4] Although macular grid laser photocoagulation[4–6] is still the gold standard treatment for macular edema secondary to BRVO, other treatment methods have been advocated including intravitreal injections of steroids[7–10] and vitrectomy with or without sheathotomy.[11–14]

Recently, an intravitreal injection of bevacizumab (Avastin; Genentech, Inc, South San Francisco, CA), a full-length recombinant monoclonal antibody against human vascular endothelial growth factor (VEGF), has been used to treat macular edema secondary to BRVO.[15–18] This therapy is widely accepted because it is known that the VEGF plays an important role in the pathogenesis of macular edema.[19–22] Long-term follow-up studies[23–26] also suggested that intravitreal

From the Department of Ophthalmology, Nagoya University Graduate School of Medicine, Nagoya, Japan.

Supported by grant-in aid 18591913 (to M.K.), 19500416 (Y.I.), and 18390466 (H.T.) from the Ministry of Education, Science, Sports and Culture, Japan.

The authors have no financial interest or conflicts of interest.

Reprint requests: Mineo Kondo, MD, PhD, Department of Ophthalmology, Nagoya University Graduate School of Medicine, 65 Tsuruma-cho, Showa-ku, Nagoya 466-8550, Japan; e-mail: kondomi@med.nagoya-u.ac.jp

bevacizumab (IVB) therapy is an effective treatment for macular edema secondary to BRVO.

In 2007, Matsumoto et al[27] reported on 3 patients with macular edema secondary to retinal vein occlusion whose edema initially responded to bevacizumab, but then showed a rebound of the macular edema. In these three patients, the degree of macular edema was greater than that before the initial bevacizumab administration. However, very little is known about the exact incidence of this rebound phenomenon and which pretreatment factors are related to this unique phenomenon.

Thus, the purpose of this study was to determine the incidence of rebound macular edema in eyes that received an IVB for macular edema secondary to BRVO. We also wanted to identify the pretreatment factors that were significantly associated with the rebound.

## Subjects and Methods

### *Subjects*

We reviewed the medical records of all patients with macular edema secondary to BRVO who had received IVB therapy at the Nagoya University Hospital from July of 2006 to April of 2009 and were followed-up for more than 6 months. Eyes that had received other treatments, for example, vitrectomy, grid laser photocoagulation, or drug injections including triamcinolone acetonide, were excluded.

The procedures used conformed to the tenets of the World Medical Association's Declaration of Helsinki. An informed consent for the IVB therapy was obtained from each of the patients before the IVB, and afterward, they were provided sufficient information on the procedures to be used. The Nagoya University Hospital Ethics Review Board approved (#09-28) this retrospective analysis of the patients' data.

### *Bevacizumab Injection*

The eyes were anesthetized with 1% topical tetracaine, and the fornices of the eyes were irrigated with 10% povidone–iodine. Each patient received an intravitreal injection of 1.25 mg/0.05 mL bevacizumab using a 30-gauge needle inserted 3.5 mm from the limbus. Antibiotics drops were given for 3 days after the IVB.

All patients received a single intravitreal injection of bevacizumab, and the effects were evaluated monthly by the best-corrected visual acuity (BCVA) and the foveal thickness determined by optical coherence tomography (OCT).

### *Best-Corrected Visual Acuity*

The BCVA was measured by a standard Japanese decimal visual acuity chart at 5 m. The decimal values were converted to the logarithm of the minimum angle of resolution units for statistical analyses.

### *Foveal Thickness*

The foveal thickness was determined by OCT (Stratus or Cirrus model; Carl Zeiss Meditec, Dublin, CA). The same OCT machine was used on the same patient. After the patients' pupils were fully dilated with 0.5% tropicamide and 0.5% phenylephrine (Mydrin-P; Santen Co, Osaka, Japan), 6 mm vertical and horizontal scans were made through the fovea. The average foveal thickness of the vertical and horizontal scans was used as the foveal thickness. We used a manual method to place the cursors on the OCT images to measure the foveal thickness[28,29] because it has been reported that the automatic measurements of the foveal thickness often failed to identify the outer border of the neural retina, especially when the Stratus model of OCT was used.[30] We have also found that our manual method is more useful when two different OCT systems were used in the same study.[31]

### *Definition of Effectiveness, Recurrence, and Rebound of Macular Edema*

A treatment was defined as effective when the OCT-determined foveal thickness had decreased by >30% after the initial bevacizumab injection. A recurrence of macular edema was defined as an increase of foveal thickness of >30% after an initial decrease of foveal thickness. A rebound of macular edema was defined as when the recurrence foveal thickness ratio (foveal thickness at the recurrence/foveal thickness at the baseline × 100) became ≥110% after an initial decrease of foveal thickness (Figure 1).

According to these definitions, we classified our 65 eyes into 4 groups (Figure 1). Group 1 included 3 eyes in which the initial bevacizumab injection was not effective. Group 2 included 21 eyes in which the initial bevacizumab injection was effective without any recurrence. Group 3 included 34 eyes in which the initial bevacizumab injection was effective, then a recurrence occurred with the recurrence ratio <110%. And Group 4 included 7 eyes in which the initial bevacizumab injection was effective, then a recurrence occurred with the recurrence ratio ≥110%, that is, a rebound.

Additional injections of bevacizumab were given only when a recurrence of macular edema or a worsening of the BCVA by ≥0.2 logarithm of the minimum angle of resolution units developed or the results of the initial injection did not reach the level considered to be effective.

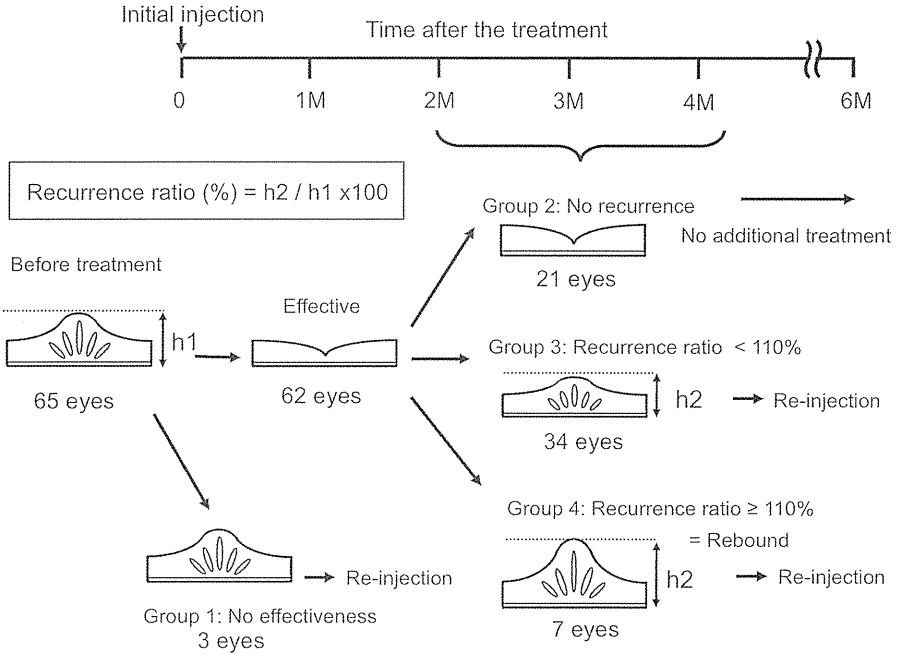


**Fig. 1.** Classification of macular edema according to the course of macular morphology obtained by OCT after IVB. Group 1 included the eyes in which the initial bevacizumab injection was not effective. Group 2 included the eyes in which the initial bevacizumab injection was effective without any recurrence thereafter. Group 3 included the eyes in which the initial bevacizumab injection was effective, and then a recurrence occurred with the recurrence ratio <110%. Group 4 included the eyes in which the initial bevacizumab injection was effective, and then a recurrence occurred with the recurrence ratio ≥110%, that is, a rebound.

*Statistical Analyses*

To identify the pretreatment factors that might influence the rebound of macular edema after the initial IVB, multivariate logistic regression analyses were performed with rebound macular edema as the dependent variable. The independent variables included patient's age, gender, presence of systemic complications, for example, hypertension, hypercholesterolemia, diabetes mellitus, pretreatment logarithm of the minimum angle of resolution visual acuity, pretreatment foveal thickness, and period from symptoms onset to the IVB.

We also performed subgroup analyses comparing the pretreatment factors presented above between Group 3 and Group 4. Differences in the patient's age, pretreatment logarithm of the minimum angle of resolution visual acuity, pretreatment foveal thickness, and period from symptoms onset to the IVB were compared using the nonparametric Mann–Whitney *U*-test. The significance of differences in gender and presence of hypertension, hypercholesterolemia, and diabetes mellitus were determined by chi-square tests.

The SPSS version 17.0J for Windows (SPSS, Inc, Chicago, IL) was used for all these statistical analyses. A $P$ value $<0.05$ was considered significant.

## Results

Intravitreal bevacizumab therapy was performed on 65 eyes of 65 consecutive patients (35 men and 30 women) whose mean ± SD age was 62.3 ± 8.6 years (range, 39–85 years). Forty-four of these patients had systemic hypertension, seven patients had diabetes mellitus without diabetic retinopathy, and six patients had hypercholesterolemia. The decimal BCVA at baseline ranged from 0.01 to 0.6, and the mean BCVA was 0.64 ± 0.33 logarithm of the minimum angle of resolution units. The mean foveal thickness was 585 ± 177 $\mu$m with a range from 244 $\mu$m to 1106 $\mu$m. The mean interval between the onset of symptoms and the IVB was 10.0 ± 8.3 weeks with a range of 2 weeks to 52 weeks. No serious systemic or local bevacizumab-related adverse events were observed in our 65 patients.

The course of macular edema after the initial IVB therapy in all 65 eyes is summarized in Figure 1. The initial injection of bevacizumab was effective in 62 of 65 eyes and was not effective in 3 eyes (4.6%; Group 1). Twenty-one eyes (32.3%) had no recurrence of macular edema after the initial reduction of the macular edema (Group 2). Thirty-four eyes (52.3%) had a recurrence of macular edema after the initial reduction of the macular edema but with a recurrence ratio <110% (Group 3). Seven eyes (10.8%) had a recurrence of macular edema after the initial reduction of the macula, and the recurrence ratio was ≥110% (Group 4). For patients in Groups 1, 3, and 4 (44 eyes, 67.7%), a second injection of IVB was performed as soon as appropriate unless the patient did not agree to a second injection.

Horizontal OCT images through the fixation point at baseline (left), at 4 weeks after the initial IVB

(middle), and at the recurrence of macular edema (right) for all 7 eyes of Group 4 are shown in Figure 2. All these 7 eyes had had an initial resolution of the macular edema at 4 weeks after the injection, but had a recurrence of the macular edema at 8 weeks to 12 weeks (mean, 9.1 weeks). The recurrence ratio (foveal thickness at the rebound/foveal thickness at the baseline × 100) ranged from 110% to 149%, and the mean was 124.6% for these 7 eyes. However, the recurrence ratio ranged from 39% to 102%, and the mean degree of recurrence was 74.7% for the 34 eyes of Group 3.

To identify the potential pretreatment factors that were associated with the rebound of macular edema, multivariate logistic regression analyses were performed on all 65 eyes, with rebound macular edema (recurrence rate ≥110%) as the dependent variable (Table 1). The results showed that a thinner pretreatment fovea (odds ratio, 0.98; 95% confidence interval, 0.96–1.00, $P = 0.063$) and a shorter interval from symptom onset to the initial injection (odds ratio, 0.47; 95% confidence interval, 0.21–1.05; $P = 0.067$) showed strong trends to be associated with the rebound of macular edema.

We next performed subgroup analyses comparing each pretreatment factor between Group 3 (recurrence rate <110%, n = 34) and Group 4 (recurrence rate ≥110, n = 7, Table 2). We found that the pretreatment fovea was significantly thinner ($P = 0.004$) in Group 4 (451 ± 70 μm) than in Group 3 (651 ± 179 μm). In addition, the interval from the symptom onset to the initiation of treatment in Group 4 (4.9 ± 2.2 weeks) was significantly shorter ($P = 0.007$) than that in Group 3 (9.1 ± 4.6 weeks). There was no significant difference in other pretreatment factors between the two groups.

To investigate the relationship between the recurrence ratio and the 2 pretreatment factors that were found to be associated with a rebound macular edema, we also plotted the recurrence ratio against the foveal

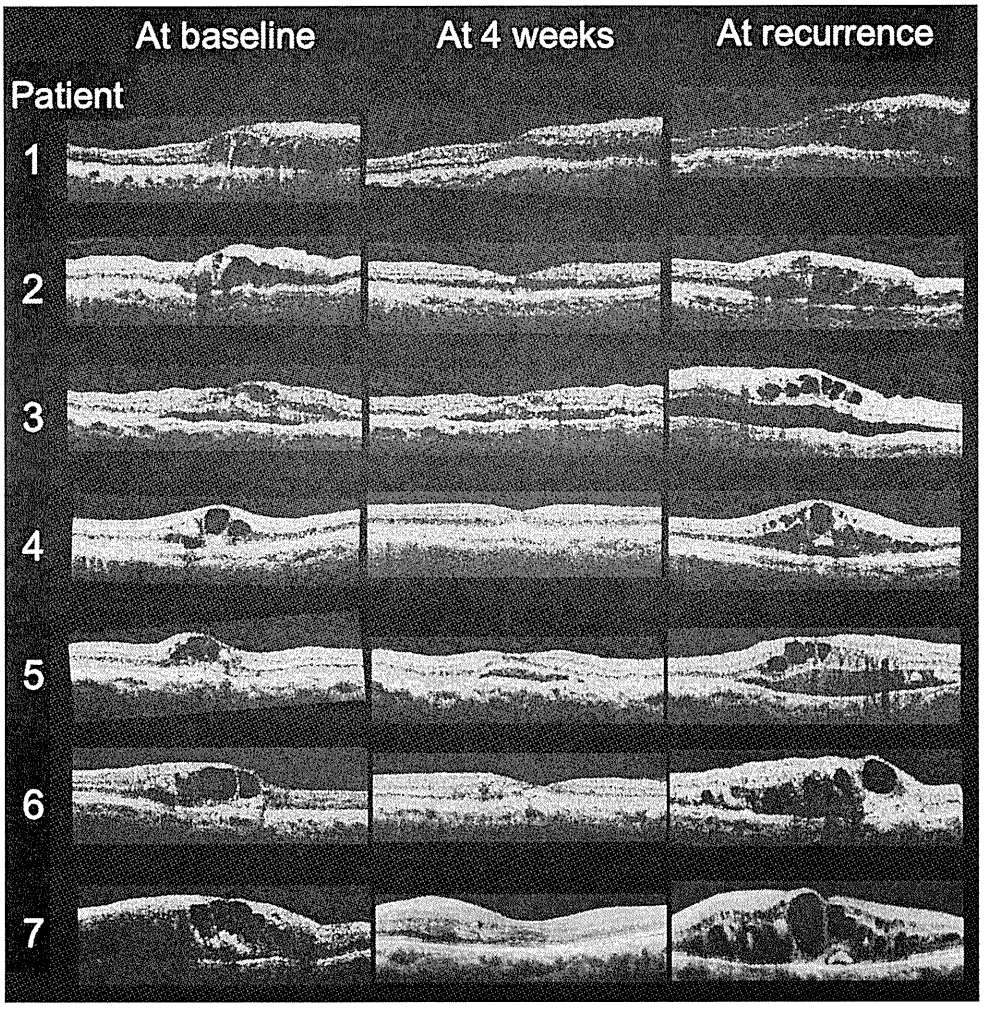


Fig. 2. Horizontal OCT images through the fixation point at baseline (left), at 4 weeks after initial bevacizumab injection (middle), and at the recurrence of macular edema (right) for all 7 eyes of Group 4 (recurrence rate ≥110%). These 7 eyes had an initial resolution of macular edema at 4 weeks after the injection but showed a recurrence of macular edema at 8 weeks or 12 weeks (mean, 9.1 weeks). At this time, their foveal thickness was ≥110% of the pretreatment thickness.

Table 1. Multivariate Logistic Regression Analysis of Pretreatment Factors Associated with the Rebound of Macular Edema Secondary to BRVO

| Factor | Odds Ratio (95% CI) | *P* |
|---|---|---|
| Age (per year) | 0.87 (0.68–1.12) | 0.285 |
| Gender (men vs. women) | 30.09 (0.6401–1417.04) | 0.083 |
| Diabetes mellitus | 20.04 (0.06–6268.55) | 0.306 |
| Hypertension | 0.35 (0.07–17.89) | 0.601 |
| Hypercholesterolemia | <0.0001 | 0.999 |
| Pretreatment visual acuity (logarithm of the minimum angle of resolution) | 0.268 (0.01–143.60) | 0.681 |
| Pretreatment foveal thickness (μm) | 0.98 (0.96–1.00) | 0.063 |
| Period from symptom onset to injection (weeks) | 0.47 (0.21–1.05) | 0.067 |

CI, confidence interval.

thickness in micrometers at the baseline (Figure 3A), and the interval from the symptom onset to the initiation of treatment in weeks (Figure 3B). In these figures, only the data of Groups 3 and 4 are plotted, because the eyes in Groups 1 and 2 did not show a recurrence of the macular edema. We found that the baseline foveal thickness for all 7 eyes with rebound (recurrence rate ≥110%) was ≤560 μm, and the interval from the symptom onset to the injection was ≤8 weeks for all 7 eyes. The intervals between the onset of symptoms and treatment in Groups 1 and 2 were 12.7 ± 10.3 and 12.5 ± 12.6 weeks, respectively.

Finally, to determine whether the rebound of macular edema resulted in a poorer post-IVB outcome, we compared the BCVA and foveal thickness at 6 months after the IVB and the total number of injections during the 6 months after the initial injection between Groups 3 and 4. The differences in these values between the 2 groups were not significant (Table 3). The reason for the low total number of injections during the 6 months in these 2 groups was that there were 14 patients (12 of Group 3 and 2 of Group 4) who did not want to receive a second injection mainly because their visual acuities were relatively maintained even though a recurrence of macular edema had occurred.

## Discussion

Our results showed that the incidence of a rebound of macular edema (recurrence ratio ≥110%) after an initial resolution after IVB was 10.8% (7 of 65 eyes). The degree of recurrence for these 7 eyes ranged from 110% to 149%, and 4 eyes had a recurrence ratio of ≥120% (Figure 3). These results indicated that the rebound of macular edema is not a rare phenomenon, and clinicians should be aware that this phenomenon can occur during the IVB therapy for macular edema associated with BRVO.

Because the rebound of macular edema is an unfavorable finding for both patients and clinicians, it is important to know what pretreatment factors were associated with the rebound. Our results using subgroup analyses demonstrated that a thinner pretreatment foveal thickness and a shorter interval from the symptom onset to the initiation of IVB were

Table 2. Comparison of Various Pretreatment Factors Between Group 3 and Group 4

| Factor | Group 3 | Group 4 | *P* |
|---|---|---|---|
| Number of eyes | 34 | 7 | |
| Age (years)* | 62.0 ± 7.4 | 57.7 ± 8.8 | 0.22 |
| Gender (men/women) | 19/15 | 5/2 | 0.37† |
| Diabetes mellitus | 4 | 2 | 0.25† |
| Hypertension | 25 | 4 | 0.39† |
| Hypercholesterolemia | 5 | 0 | 0.28† |
| Pretreatment visual acuity (logarithm of the minimum angle of resolution)* | 0.55 ± 0.24 | 0.68 ± 0.18 | 0.1 |
| Pretreatment foveal thickness (μm)* | 651 ± 179 | 451 ± 70 | 0.004 |
| Period from symptom onset to injection (weeks)* | 9.1 ± 4.6 | 4.9 ± 2.2 | |

Group 3 = eyes with recurrence ratio <110%. Group 4 = eyes with recurrence ratio. Differences between two groups were analyzed using a nonparametric Mann–Whitney *U*-test.

*Data are expressed as the mean ± SD.

†Differences between the two groups were analyzed using a chi-square test.

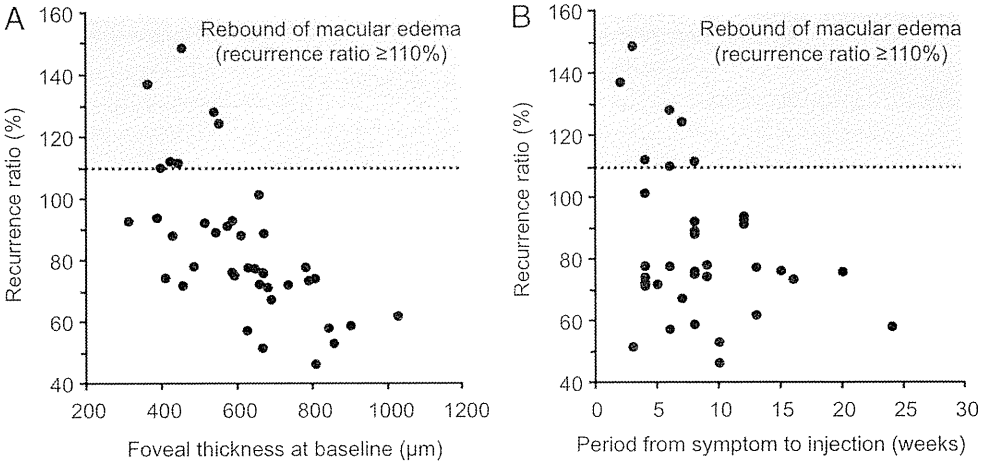


**Fig. 3.** Relationship between the recurrence ratio (foveal thickness at the rebound/foveal thickness at the baseline × 100) and 2 pretreatment factors for the 41 eyes of Groups 3 and 4. **A.** The recurrence ratio plotted against the foveal thickness at the baseline (in micrometers). **B.** The recurrence ratio plotted against the period from symptom onset to the initiation of treatment (weeks). Gray areas show the eyes with recurrence ratio ≥110%, that is, a rebound.

significantly associated with a rebound of macular edema. Interestingly, all 7 eyes that had a rebound of macular edema received the IVB therapy within 8 weeks of the onset of the symptoms (Figure 3B). These results suggest that the rebound of macular edema was more likely to occur when the IVB therapy was initiated at a relatively early stage of the macular edema before the edema had reached the maximum degree of edema in eyes with a BRVO. In other words, the rebound of macular edema may be more likely to occur in eyes in which the macular edema might have worsened if they had not received the IVB therapy during its natural course.

However, other factors may be involved in the mechanism for the rebound of macular edema after the IVB therapy, because 1 of 3 patients with rebound macular edema reported by Matsumoto et al[27] had received the IVB therapy 22 months after the diagnosis. They hypothesized that the inhibition of the VEGF pathway by IVB may upregulate VEGF receptors within the retina of the patients, and this upregulation may make the endothelial cells more sensitive to the VEGF that are already upregulated because of the underlying ischemic state.[27] Quantitative analysis of the changes in the expression of the VEGF receptors at various times after IVB therapy in an animal model of BRVO may answer this question.

We also studied whether there was any difference in the post-IVB outcomes between the eyes with and without rebound (Group 3 vs. Group 4), and we found that there was no significant difference in any of the post-IVB outcome values (Table 3). These findings suggest that the eyes with rebound macular edema do not necessarily result in poorer visual outcome than eyes without a rebound. However, we hesitate to draw this conclusion based on our results, because of the few eyes in Group 4 and the high withdrawal rate for additional injections in Groups 3 and 4. The reason for the high withdraw rate was because the decision to give additional injections was done not only by the data of foveal

Table 3. Comparison of Posttreatment Values Between Group 3 and Group 4

| Posttreatment Values | Group 3 | Group 4 | *P* |
|---|---|---|---|
| BCVA at recurrence (logarithm of the minimum angle of resolution) | 0.27 ± 0.21 | 0.44 ± 0.30 | 0.15 |
| Changes in BCVA between baseline and recurrence (logarithm of the minimum angle of resolution) | 0.33 ± 0.26 | 0.28 ± 0.19 | 0.85 |
| Number of injections within 6 months | 1.8 ± 0.7 | 2.0 ± 0.8 | 0.50 |
| BCVA at 6 months after initial injection (logarithm of the minimum angle of resolution) | 0.22 ± 0.21 | 0.35 ± 0.25 | 0.16 |
| Changes in BCVA between baseline and 6 months after initial injection (logarithm of the minimum angle of resolution) | 0.35 ± 0.27 | 0.33 ± 0.14 | 0.89 |
| Foveal thickness at 6 months after initial injection (μm) | 400 ± 150 | 375 ± 170 | 0.59 |

Data are expressed as mean ± SD. Differences between two groups were analyzed using a nonparametric Mann–Whitney *U*-test.
VA, visual acuity.

thickness and visual acuity but also by the patient's approval. Thus, few eyes and high withdrawal rate for additional injections were limitations of our study.

The incidence of rebound macular edema in BRVO was 10.8%. However, this percentage may change because of the interval of the follow-up period. We followed-up our patients monthly and performed a second injection immediately when a recurrence was detected. It is possible that if our follow-up interval was shorter, for example, every week or every 2 weeks, then we might have detected a recurrence earlier and performed a second injection at an earlier stage of recurrence, resulting in lower incidence of rebound macular edema. The incidence of rebound macular edema can also change because of the period from symptom onset to the injection. If we initiated the IVB therapy after a 2- to 3-month observational period, then the incidence of rebound macular edema might have been lower than what we found (Figure 3B). In addition, the incidence of rebound macular edema can also change if multiple injections (e.g., three times monthly) had been adopted at the initial injection.

Finally, there is still discussion about when the IVB therapy should be initiated in eyes with macular edema secondary to BRVO. It is widely recommended that any invasive treatments for macular edema secondary to BRVO should be initiated at least 2 months to 3 months after the symptom onset because spontaneous resolution of macular edema can occur mostly within this period.[4,23,24] We did not set any observational window before the initiation of IVB. However, based on our results, we now believe that it is reasonable to wait at least 2 months after the onset to begin the IVB, because in addition to excluding eyes with spontaneous resolution, a rebound of macular edema may be avoided by waiting 2 months after the symptom onset.

**Key words:** branch retinal vein occlusion, macular edema, bevacizumab, vascular endothelial growth factor, rebound.

## Acknowledgments

The authors thank Professor Duco Hamasaki of Bascom Palmer Eye Institute for discussions and editing the final version of the manuscript.

## References

1. Gutman FA. Macular edema in branch retinal vein occlusion: prognosis and management. Trans Am Acad Ophthalmol Otolaryngol 1977;83:488–495.
2. Hoerauf H. Branch retinal vein occlusion. In: Joussen AM, Gardner TW, Kirchhof B, Ryan SJ. eds. Retinal Vascular Disease. Philadelphia, PA: Springer; 2007:467–506.
3. Rehak J, Rehak M. Branch retinal vein occlusion: pathogenesis, visual prognosis, and treatment modalities. Curr Eye Res 2008;33:111–131.
4. The Branch Vein Occlusion Study Group. Argon laser photocoagulation for macular edema in branch vein occlusion. Am J Ophthalmol 1984;98:271–282.
5. Arnarsson A, Stefánsson E. Laser treatment and the mechanism of edema reduction in branch retinal vein occlusion. Invest Ophthalmol Vis Sci 2000;41:877–879.
6. McIntosh RL, Mohamed Q, Saw SM, Wong TY. Interventions for branch retinal vein occlusion: an evidence-based systematic review. Ophthalmology 2007;114:835–854.
7. Jonas JB, Akkoyun I, Kamppeter B, Kreissig I, Degenring RF. Branch retinal vein occlusion treated by intravitreal triamcinolone acetonide. Eye 2005;19:65–71.
8. Avitabile T, Longo A, Reibaldi A. Intravitreal triamcinolone compared with macular laser grid photocoagulation for the treatment of cystoid macular edema. Am J Ophthalmol 2005; 140:695–702.
9. Ozkiris A, Evereklioglu C, Erkilic K, Dogan H. Intravitreal triamcinolone acetonide for treatment of persistent macular oedema in branch retinal vein occlusion. Eye 2006;20: 13–17.
10. Scott IU, Ip MS, VanVeldhuisen PC, et al.; SCORE Study Research Group. A randomized trial comparing the efficacy and safety of intravitreal triamcinolone with standard care to treat vision loss associated with macular edema secondary to branch retinal vein occlusion: the Standard Care vs Corticosteroid for Retinal Vein Occlusion (SCORE) study report 6. Arch Ophthalmol 2009;127:1115–1128.
11. Osterloh MD, Charles S. Surgical decompression of branch retinal vein occlusions. Arch Ophthalmol 1988;106:1469–1471.
12. Opremcak EM, Bruce RA. Surgical decompression of branch retinal vein occlusion via arteriovenous crossing sheathotomy: a prospective review of 15 cases. Retina 1999; 19:1–5.
13. Yamamoto S, Saito W, Yagi F, Takeuchi S, Sato E, Mizunoya S. Vitrectomy with or without arteriovenous adventitial sheathotomy for macular edema associated with branch retinal vein occlusion. Am J Ophthalmol 2004;138:907–914.
14. Kumagai K, Furukawa M, Ogino N, Uemura A, Larson E. Long-term outcomes of vitrectomy with or without arteriovenous sheathotomy in branch retinal vein occlusion. Retina 2007;27:49–54.
15. Rabena MD, Pieramici DJ, Castellarin AA, Nasir MA, Avery RL. Intravitreal bevacizumab (Avastin) in the treatment of macular edema secondary to branch retinal vein occlusion. Retina 2007; 27:419–425.
16. Kreutzer TC, Alge CS, Wolf AH, et al. Intravitreal bevacizumab for the treatment of macular oedema secondary to branch retinal vein occlusion. Br J Ophthalmol 2008;92:351–355.
17. Wu L, Arevalo JF, Roca JA, et al; Pan-American Collaborative Retina Study Group (PACORES). Comparison of two doses of intravitreal bevacizumab (Avastin) for treatment of macular edema secondary to branch retinal vein occlusion: results from the Pan-American Collaborative Retina Study Group at 6 months of follow-up. Retina 2008;28:212–219.
18. Kriechbaum K, Michels S, Prager F, et al. Intravitreal Avastin for macular oedema secondary to retinal vein occlusion: a prospective study. Br J Ophthalmol 2008;92:518–522.
19. Noma H, Minamoto A, Funatsu H, et al. Intravitreal levels of vascular endothelial growth factor and interleukin-6 are correlated with macular edema in branch retinal vein occlusion. Graefes Arch Clin Exp Ophthalmol 2006;244:309–315.

20. Noma H, Funatsu H, Yamasaki M, et al. Aqueous humour levels of cytokines are correlated to vitreous levels and severity of macular oedema in branch retinal vein occlusion. Eye 2008;22:42–48.
21. Adamis AP, Shima DT. The role of vascular endothelial growth factor in ocular health and disease. Retina 2005;25:111–118.
22. Campochiaro PA. Seeing the light: new insights into the molecular pathogenesis of retinal diseases. J Cell Physiol 2007; 213:348–354.
23. Jaissle GB, Leitritz M, Gelisken F, Ziemssen F, Bartz-Schmidt KU, Szurman P. One-year results after intravitreal bevacizumab therapy for macular edema secondary to branch retinal vein occlusion. Graefes Arch Clin Exp Ophthalmol 2009;247:27–33.
24. Prager F, Michels S, Kriechbaum K, et al. Intravitreal bevacizumab (Avastin) for macular edema secondary to retinal vein occlusion—twelve-month results of a prospective clinical trial. Br J Ophthalmol 2008;93:452–456.
25. Kondo M, Kondo N, Ito Y, et al. Intravitreal injection of bevacizumab for macular edema secondary to BRVO: results after 12-months and multiple regression analysis. Retina 2009; 29:1242–1248.
26. Wu L, Arevalo JF, Berrocal MH, et al. Comparison of two doses of intravitreal bevacizumab as primary treatment for macular edema secondary to branch retinal vein occlusions: results of the Pan American Collaborative Retina Study Group at 24 months. Retina 2009;29:1396–1403.
27. Matsumoto Y, Freund KB, Peiretti E, Cooney MJ, Ferrara DC, Yannuzzi LA. Rebound macular edema following bevacizumab (Avastin) therapy for retinal venous occlusive disease. Retina 2007;27:426–431.
28. Ishikawa K, Kondo M, Ito Y, et al. Correlation between focal macular electroretinograms and angiographic findings after photodynamic therapy. Invest Ophthalmol Vis Sci 2007;48: 2254–2259.
29. Sugita T, Kondo M, Piao CH, Ito Y, Terasaki H. Correlation between macular volume and focal macular electroretinogram in patients with retinitis pigmentosa. Invest Ophthalmol Vis Sci 2008;49:3551–3558.
30. Costa RA, Calucci D, Skaf M, et al. Optical coherence tomography 3: automatic delineation of the outer neural retinal boundary and its influence on retinal thickness measurements. Invest Ophthalmol Vis Sci 2004;45:2399–2406.
31. Kakinoki M, Sawada O, Sawada T, Kawamura H, Ohji M. Comparison of macular thickness between Cirrus HD-OCT and Stratus OCT. Ophthalmic Surg Lasers Imaging 2009;40:135–140.

# A case of aniridia with unilateral Peters anomaly

Mayu Sawada, MD,[a] Miho Sato, MD, PhD,[a] Akiko Hikoya, MD, PhD,[a] Chunxia Wang, MD, PhD,[a,b] Shinsei Minoshima, PhD,[b] Noriyuki Azuma, MD, PhD,[c] and Yoshihiro Hotta, MD, PhD[a]

Aniridia is an autosomal-dominant, panocular, congenital anomaly transmitted with high penetrance and largely caused by mutations in the *PAX6* gene. Although Peters anomaly may also be caused by mutations in *PAX6*, there has not to our knowledge been a report of aniridia associated with lens displacement into the anterior chamber and lenticular-corneal attachment. We report a child with aniridia and Peters anomaly associated with a *PAX6* gene mutation.

## Case Report

A 9-day-old boy was referred to the Department of Ophthalmology, Hamamatsu University Hospital, for an opacity noted in the left eye. He had been born via vacuum-assisted vaginal delivery with a birth weight of 2,222 g. An examination under anesthesia was performed with oral triclofos sodium sedation. Slit-lamp examination revealed bilateral aniridia. The left lens was dislocated into the anterior chamber (Figure 1A) and adherent to the cornea, with corneal opacification at the area of contact. IOP was 12 mm Hg in the right eye and 10 mm Hg in the left by Tono-Pen (Reichert Technologies, Depew, NY). Fundus examination revealed macular hypoplasia. Ultrasound biomicroscopy (TOMEY UD-6000, Tokyo, Japan) confirmed that the left lens was dislocated into the anterior chamber, thicker, and more spherical than the right lens and adherent to the cornea (Figure 1B and 1C). Slit-lamp examination of his parents' eyes revealed no abnormality.

On examination at 2 months of age, bilateral macular hypoplasia was confirmed, and horizontal pendular nystagmus was detected. At 4 months of age, visual acuity was 0.65 cycles/degree in the right eye at 38 cm with the use of Teller Acuity Cards (Stereo Optical Co., Chicago, IL), with strong resistance to occlusion of the right eye.

At age 2.5 years, the corneal opacity of the patient's left eye had not changed, but the lens opacity had worsened, affecting cosmesis. Lensectomy was performed by a 2-port procedure under general anesthesia. At surgery, the lens was found to be firmly attached to the cornea,

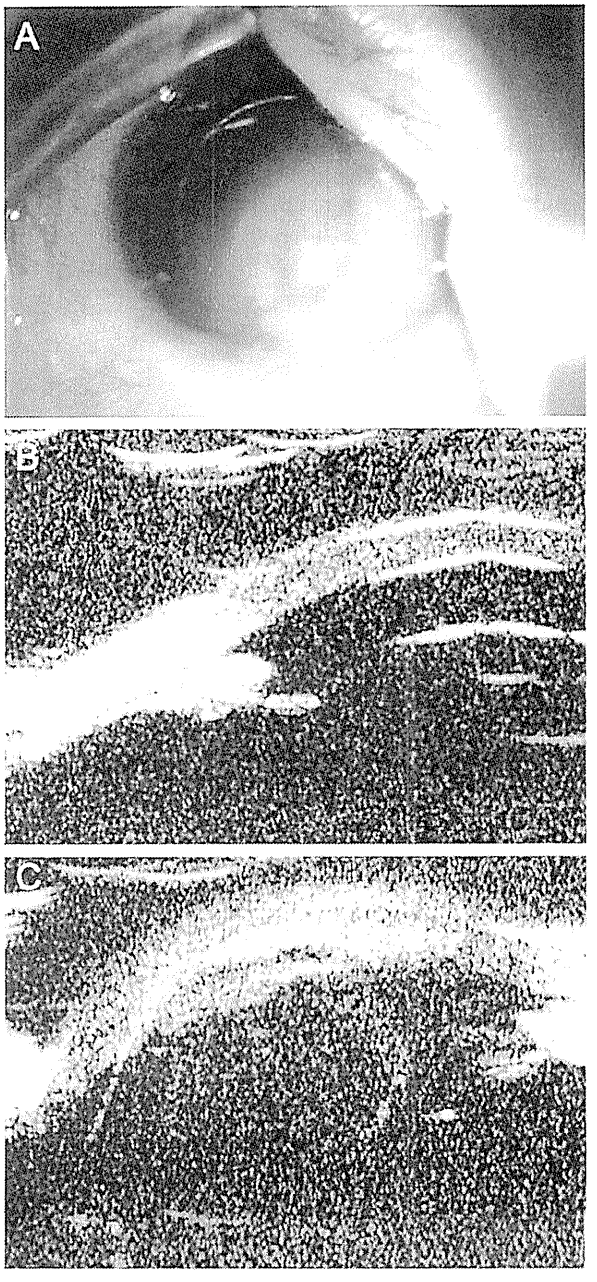


FIG 1. Clinical photographs and ultrasound of a 9-day-old boy with bilateral aniridia and left lens dislocation. A, Photograph of the anterior segment of the left eye: the lens appears to be adherent to the cornea, which is opacified at the site of attachment. Ultrasound biomicroscopic images of the right (B) and left (C) eyes showing absence of most of the iris in both: the left lens is thicker and more spherical than the right. Corneal density appears higher in the area of attachment.

*Author affiliations: [a]Department of Ophthalmology, Hamamatsu University School of Medicine, Hamamatsu, Japan; [b]Department of Medical Photobiology, Photon Medical Research Center, Hamamatsu University School of Medicine; and [c]Department of Ophthalmology, National Center for Child Health and Development, Tokyo, Japan*

*Submitted June 7, 2010.*

*Revision accepted November 6, 2010.*

*Reprint requests: Yoshihiro Hotta, MD, Department of Ophthalmology, Hamamatsu University School of Medicine, Higashi-ku, 1-20-1 Handayama, Hamamatsu, 431-3192, Japan (email: hotta@hama-med.ac.jp).*

*J AAPOS 2011;15:104-106.*



*1091-8531/$36.00*

*doi:10.1016/j.jaapos.2010.11.006*

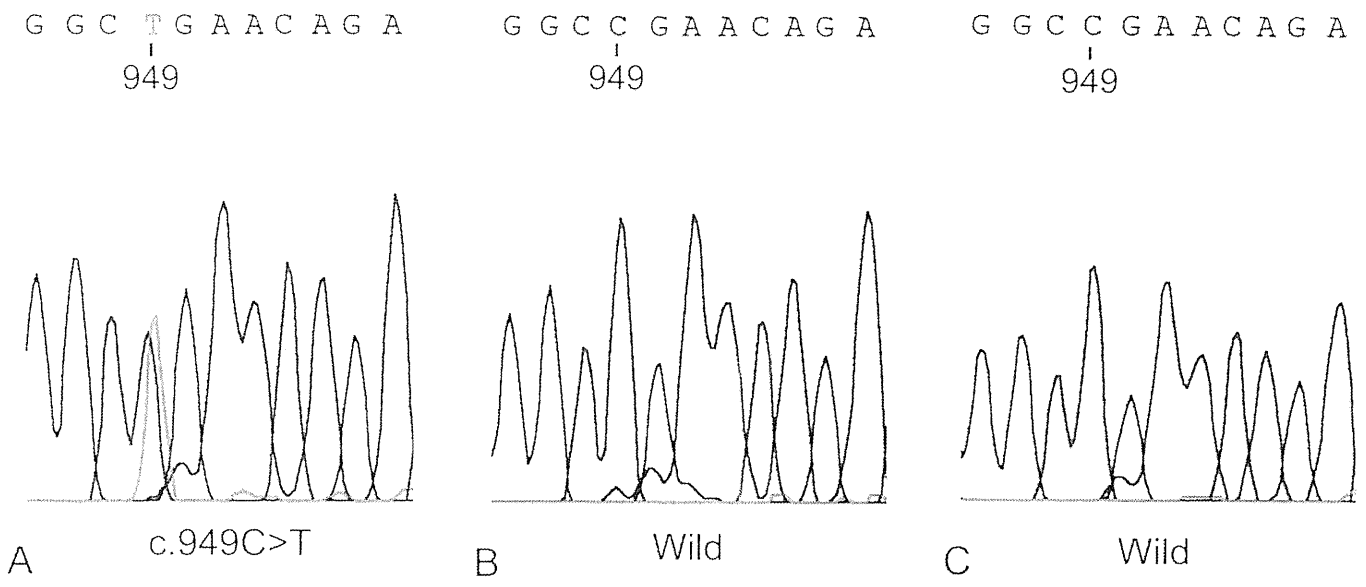


FIG 2. The patient had a nonsense mutation, C949T (R317X), in exon 11 of the *PAX6* gene (A). His parents, father (B), mother (C), did not have the mutation in exon 11 of the *PAX6* gene.

and the anterior capsule could not be distinguished from Descemet's membrane. Postoperatively, the corneal opacity increased slightly, and the IOP remained less than 20 mm Hg. At the age of 2 11/12 years, the patient recognized Landolt C optotypes with visual angle of 0.1° at 1.5 m (20/667) with his right eye but not with his uncorrected left eye. Amblyopia therapy was not initiated because of poor prognosis and infeasibility of contact lens wear.

After informed consent was obtained, genetic testing was performed, with the procedures described in detail elsewhere.[1] In brief, the 13 exons and surrounding intronic areas of the *PAX6* gene were amplified by polymerase chain reaction and directly sequenced. The patient had a nonsense mutation, C949T (R317X), in exon 11 of the *PAX6* gene (Figure 2A). The mutation was not detected in his parents (Figure 2B and 2C).

## Discussion

*Aniridia is most often* caused by mutations in the *PAX6* gene.[2] The R317X mutation of *PAX6* in our patient has also been reported in white, East Indian, and Chinese patients.[3-5] The absence of both the ocular abnormalities and the mutation in his parents suggested a de novo mutation. The parents were therefore informed that the risk of the aniridia in a future child was very low.

Aniridia may be accompanied by various ocular changes, including congenital cataract, subluxated lenses, glaucoma, and macular hypoplasia.[6] Various corneal opacities, including possible Peters anomaly accompanied with aniridia, have been reported.[7] The most common congenital cataract in aniridia is anterior pyramidal, which is thought to be a forme fruste of Peters. The pyramid can even be attached to the cornea. Lens subluxation in aniridia is rare[8]; we found no reports of unilateral Peters anomaly associated with aniridia or of unilateral lens dislocation into the anterior chamber and lenticular-corneal attachment associated with aniridia.

The total lens malposition may be caused by an incomplete separation of the lens from the surface ectoderm at an early stage of development or a secondary adhesion of a lens dislocated lens into the anterior chamber. Embryologically, the detachment of the lens vesicle from the surface ectoderm is the initial event leading to the formation of the chambers of the eye.

Because haploinsufficiency of the *PAX6* gene can cause congenital cataracts and Peters anomaly, which possibly result from faulty keratolenticular separation, the mutation may also cause total lens malposition by an incomplete keratolenticular separation. It is also possible that a dislocated lens that was initially located in the posterior chamber moved into the anterior chamber and attached to the cornea because the iris barrier between the anterior and posterior chamber was absent. If this were the mechanism, however, then anterior lens dislocation would be far more commonly observed in patients with aniridia. Although secondary adhesion of the lens may have possibly occurred, the intraoperative findings were most consistent with the hypothesis that lens malposition was caused by an incomplete separation of the lens from the surface ectoderm.

## Literature Search

PubMed was searched for the following terms: *aniridia* AND *Peters anomaly* and combinations of *aniridia*, *subluxated lens*, *malposition*, and *PAX6* or *Peters*.

### References

1. Kawano T, Wang C, Hotta Y, Sato M, Iwata-Amano E, Hikoya A, et al. Three novel mutations of the *PAX6* gene in Japanese aniridia patients. J Hum Genet 2007;52:571-4.

2. Prosser J, van Heyningen V. PAX6 mutations reviewed. Hum Mutat 1998;11:93-108.
3. Chauhan BK, Yang Y, Cveklová K, Cvekl A. Functional properties of natural human PAX6 and PAX6(5a) mutants. Invest Ophthalmol Vis Sci 2004;45:385-92.
4. Dharmaraj N, Reddy A, Kiran V, Mandal A, Panicker S, Chakrabarti S. PAX6 gene mutations and genotype-phenotype correlations in sporadic cases of aniridia from India. Opthalmic Genet 2003;24:161-5.
5. Chien YH, Huang HP, Hwu WL, Chien YH, Chang TC, Lee NC. Eye anomalies and neurological manifestations in patients with PAX6 mutations. Mol Vis 2009;15:2139-45.
6. Nelson LB, Spaeth GL, Nowinski TS, Margo CE, Jackson L. Aniridia: A review. Surv Ophthalmol 1984;28:621-42.
7. Beauchamp GR. Anterior segment dysgenesis keratolenticular adhesion and aniridia. J Pediatr Ophthalmol Strabismus 1980;17:55-8.
8. David R, MacBeath L, Jenkins T. Aniridia associated with microcornea and subluxated lenses. Br J Ophthalmol 1978;62:118-21.

総説

# 間欠性外斜視の評価と分類

佐藤美保

〔要　約〕

間欠性外斜視は，アジア人に最も多い斜視の一つである。小児では，整容面，立体視や視力といった視機能が問題となり，成人では，整容面と複視が問題となる。遠見と近見の眼位の差で分類し，術式の選択に役立てる。手術は4歳以降で行うことが勧められ，外直筋後転術，内直筋前転術の単独あるいは組み合わせが行われる。整容的な治癒をえるためには，斜視角が15プリズム以内に収まることが重要であるが，斜視角だけでなく，コントロール状態が良好であることが必要である。コントロール状態を評価するために，Newcastle Control Scoreを用いると良い。

## はじめに

間欠性外斜視（intermittent exotropia: 通常X（T）と記載する。（表1）[1]）とは，外斜視と外斜位をくりかえすものでアジア人では最も頻度の高い斜視である。斜位のときには，両眼視機能がよいが，斜視のときには抑制がかかるか複視を自覚する。手術によって眼位も両眼視機能も改善することが多いが，術後の再発がしばしばみられることから，治療のタイミングや治療方法が議論となる。大切なことは，正しく病態の評価を行ったうえで治療することであり，そうすれば高い患者満足度が得られる。

表1　一般的な斜視の記載方法

| | 斜位 | | 斜視 | | 間欠性斜視 | |
|---|---|---|---|---|---|---|
| | 近見 | 遠見 | 近見 | 遠見 | 近見 | 遠見 |
| 内方偏位 | E′ | E | ET′ | ET | E（T）′ | E（T） |
| 外方偏位 | X′ | X | XT′ | XT | X（T）′ | X（T） |

E: Esophoria 内斜位，ET: Esotropia 内斜視
X: Exophoria 外斜位，XT: Exotropia 外斜視
「′」は近見眼位を意味する
（　）でくくると間欠性を意味する

## Ⅰ．間欠性外斜視の症状

小児期に発症した間欠性外斜視では，外斜視のときには片眼が抑制されて複視を自覚しないが，斜位のときには抑制はかからず良好な立体視を示すことが多い。そのため多くの場合，見え方に関する症状を自覚することはなく，家族が外見から斜視に気づき来院することが多い。また戸外の明るい所に行くと，片目を閉じてしまい見づらそうにすることがある。本人が斜視に気づく年齢に達し，鏡や写真で自分を見たり，他人から指摘されたりして斜視を自覚するようになると，意識して両眼で見ようとすることが多い。一方，近見で斜視になり自分でコントロールができない場合，複視や眼精疲労を自覚することがある。遠方視で目立つ斜視だと，対人関係に自信をなくしたり，就職で不利な評価をうけたりして社会生活上の問題となる。患者のなかには，整容的に気にしていることは恥ずかしいと感じる人もあり，訴えが曖昧なことがある。その点に配慮したうえで診療に当たることが必要である。

佐藤　美保：浜松医科大学眼科